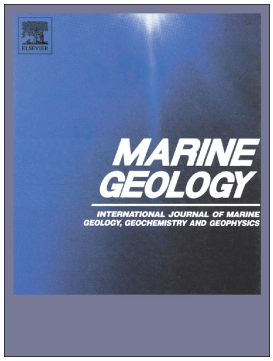

Provenance and depositional variability of the Thin Mud Facies in the lower Ganges-Brahmaputra delta, West Bengal Sundarbans, India

R.P. Flood, I.D. Barr, G.J. Weltje, S. Roberson, M.I. Russell, J. Meneely, J.D. Orford

PII: S0025-3227(16)30303-6
DOI: doi: 10.1016/j.margeo.2017.09.001
Reference: MARGO 5683

To appear in: *Marine Geology*

Received date: 16 November 2016
Revised date: 30 August 2017
Accepted date: 5 September 2017

Please cite this article as: R.P. Flood, I.D. Barr, G.J. Weltje, S. Roberson, M.I. Russell, J. Meneely, J.D. Orford , Provenance and depositional variability of the Thin Mud Facies in the lower Ganges-Brahmaputra delta, West Bengal Sundarbans, India, *Marine Geology* (2017), doi: 10.1016/j.margeo.2017.09.001

Provenance and depositional variability of the Thin Mud Facies in the lower Ganges-Brahmaputra delta, West Bengal Sundarbans, India

R.P., Flood[1,*], I.D., Barr[1], G.J., Weltje[2], S., Roberson[3], M.I., Russell[1], J. Meneely[1], J.D., Orford[1]

[1]School of Natural and Built Environment, Queen's University Belfast, Belfast, BT7 1NN, Northern Ireland, UK

[2]Department of Earth and Environmental Sciences, Geology Division, University of Leuven, Celestijnenlaan 200E, 3001 Leuven-Heverlee, Belgium

[3]Geological Survey of Northern Ireland, Dundonald House, Upper Newtownards Road, Belfast BT4 3SB, Northern Ireland, UK

[*]Corresponding author. Present address: Department of Petroleum and Energy Engineering, The American University in Cairo, New Cairo 11835, Arab Republic of Egypt. Email address: rory.flood@aucegypt.edu

Keywords: Ganges-Brahmaputra delta; West Bengal Sundarbans; grain-size; XRD; XRF; mineralogy; geochemistry; weathering; provenance.

ABSTRACT

The Sundarbans is one of the largest coastal wetland sites in the world and covers an area of approximately one million hectares of the western delta of the Ganges and Brahmaputra (G-B) rivers (located across Bangladesh and India). Since the late Holocene, the western delta has not been directly fluvially sourced, due to the Ganges shift to the east (present-day Bangladesh). The depositional facies (Thin Mud

Facies) of the late-Holocene abandoned western region (The Sundarbans) is derived from dominant estuary-tidal dynamics, however the provenance of the associated TMF sedimentation in this far western zone (Indian Sundarbans *per se*) is as yet equivocal. In this study, sediment cores from the Indian Sundarbans (Saptamukhi-Thakuran estuary) were closely examined for grain-size distributions (GSDs), mineralogy through X-ray diffraction (XRD), and geochemistry with X-ray fluorescence (XRF). The TMF in the West Bengal Sundarbans has been determined to show intensively weathered, terrestrial sediment, derived principally from the Ganges Alluvial Plain (GAP). There is a predominance of quartz, mica and clay minerals, with quartz interpreted as a product of low-relief tropical weathering sourced via the G-B Rivers draining the Himalayas. Lithofacies interpreted through GSD analysis of the TMF is indicative of a muddy tidal flat environment with aggradation and a general fining-up trend between the adjacent estuaries. The sediment provenance indicates a continuing G-B sediment source, which moves westward along the Bay of Bengal, from the active delta front and is then reworked over the far-western abandoned delta by tidal–estuarine forcing.

1. INTRODUCTION

The Indian Sundarbans comprises just over 400,000 hectares of mangrove land cover in the western sector of the Ganges-Brahmaputra (G-B) delta, and is cross-cut by a number of approximately north-south estuarine channels; the Mooriganga, Saptamukhi, Thakuran, Matla, Bidya, Gosaba, and Haribhanga (Fig. 1). The overall morphology of the far-western G-B delta reflects that of a tide-dominated system. Depositionally it falls on the extreme of a west-east continuum of tidal, mixed tidal-fluvial, and purely fluvial in the contemporary G-B river mouth estuary (Rogers et al., 2013). The eastern sector of the G-B delta comprises the fluvially dominated system, where fluvially-driven shoreline progradation occurred following the joining of the Ganges and Brahmaputra Rivers (Allison, 1998a), while the older abandoned part of the delta, in the west, comprises the non-fluvially dominated system (no longer directly linked fluvially to the G-B River sources) (Rogers et al., 2013). This western part of the delta, which underlies the present day Indian Sundarbans, was fluvially abandoned prior to c. 5000 cal yr BP, as the Ganges River migrated eastward towards its present position (Goodbred and Kuehl, 2000a; Sarkar et al., 2009). Over the last 4,000 yrs, the West Bengal Sundarbans area is thought to be estuary-tidal in terms of process domination, leading to the deposition of what is termed the "Thin Mud Facies" (TMF: Goodbred and Kuehl, 2000a). The origin of TMF sediments in what is now the Bangladesh Sundarbans, is considered to be related to reworking of G-B sourced muds from the delta front (Allison et al., 2003; Rogers et al., 2013), but a similar provenance for the Indian Sundarbans TMF has still to be substantiated. The western extent of the G-B delta is now considered to be undergoing net delta front erosion as a result of eustatic sea-level rise and tectonic subsidence (Allison, 1998b; Allison et al., 2003) and, by inference, is seen as one

possible source for the extreme western TMF. This paper aims to establish sedimentary depositional processes and provenance in the West Bengal Sundarbans during the last 4-5,000 yrs, and addresses the potential sources of sediment in the far "abandoned" western sector of the G-B delta system, by analysing sedimentary cores from three deltaic islands in the far-western Sundarbans; Lothian, Dhanchi, and Gplot, shown in Fig. 1(ii).

2. LATE-PLEISTOCENE AND HOLOCENE SEDIMENTARY FACIES OF THE LOWER GANGES-BRAHMAPUTRA DELTA

2.1. Background

The majority of studies on the Quaternary stratigraphy and sedimentary facies of the Ganges-Brahmaputra (G-B) system have determined the appropriate broad-scale sedimentary facies models (e.g., Morgan and McIntire, 1959; Coleman, 1969; Umitsu, 1987, 1993; Kuehl et al., 1989; Johnson and Alam, 1991; Lindsay et al., 1991; Curray, 1991; Johnson, 1994; Hait et al., 1996; Kuehl et al., 1997; Hübscher et al., 1998; Stanley and Hait, 2000; Goodbred and Kuehl, 2000a, 2000b; Goodbred et al., 2003; Allison et al., 2003; Sarkar et al., 2009). These studies show variability in the use of facies descriptions for the G-B delta and these tend to follow the broader scale late Quaternary evolution of the delta (e.g., Goodbred and Kuehl, 2000a), or Holocene evolution of the lower delta plain (e.g., Allison et al., 2003). In terms of the entire G-B delta, the oldest stratigraphic units are dated from 18,000 cal yr BP and consist of coarse channel sands, indicative of lowstand alluvial valleys and oxidized laterites associated with subaerial weather exposure (Goodbred et al., 2003). Fining-up of the channel sands and a silty mud unit with wood and marine fossils is understood to have taken place from 10,000–11,000 cal yr BP, and has been

interpreted as a mangrove-colonized coastal plain (Goodbred et al., 2003). From c. 11,000–3,000 cal yr BP, muddy fluvial sands of the mid-Holocene prograding river channels overlay these coastal facies, with the upper delta stratigraphy consisting of single or multiple fining-up sand sequences that are locally interspersed with silty floodplain deposits. The late Quaternary stratigraphic facies of the G-B delta have been broken down into six principal groups by Goodbred and Kuehl (2000a): Oxidised Facies (OF), Sand Facies (SF), Lower Delta Mud Facies (LDMF), Muddy Sand Facies (MSF), Sylhet Mud Facies (SMF), and Thin Mud Facies (TMF). This description of stratigraphic facies succession has been further developed by Allison et al. (2003) to look specifically at the lower delta plain stratigraphy. The lower delta plain stratigraphy has been further divided into five units: Muddy Sand (MS), Mottled Mud (MM), Interbedded Mud (IM), Laminated Sand (LS), and Peaty Mud (PM) (Allison et al., 2003). The fining up in grain size from the MS to IM/MM, located west of the active G-B river mouths is attributed to either older phases or multiple phases of progradation of the lower delta plain (Allison et al., 2003). Subaqueous shoal sedimentation has been linked to the MSF as a result of the reduced mud content and cross-stratification associated with bedload transport (Allison et al., 2003). Current energies have been found to diminish in the preserved upward section of the core sections examined by Allison et al. (2003) which allow for enhanced deposition of mud, illustrating this upward fining of the sequences.

2.2. Thin Mud Facies of the Ganges-Brahmaputra delta

Goodbred and Kuehl (2000a) describe the TMF as representing the cap unit of coarser underlying facies units throughout the Bengal Basin, consisting of overbank deposits of the modern and recent floodplain system. Deposition of this facies unit

took place from approximately 5000 cal yr BP to present, and is present within a depth of 5-7 m to the surface of the G-B delta. This unit is generally poorly preserved in the deeper stratigraphy indicative of rapid channel migration and frequent avulsion and subsequent removal. As outlined by Allison et al. (2003) the TMF and surface sediments of the lower delta plain tend to be very homogenous silts to clayey silts with the Sundarbans in the west presenting slightly finer material on average in comparison to that of the eastern delta. The lithostratigraphy of the near surface sediments appears to be homogenous with a network of mangrove roots at a depth of 3–4 m below the surface. Bed thicknesses tend to range from 3-10 cm, with a series of alternating layers of clay dominant and clay-deficient silts.

The TMF is understood to be found in floodplain environments and absent near active fluvial channels and is interpreted as abandoned floodplain overbank deposits (Goodbred and Kuehl, 2000a). In contrast to Goodbred and Kuehl's observations of the TMF as a product of abandoned floodplain and overbank deposits, Allison et al. (2003) regard the source of TMF sediments as reworked Bengal Bay nearshore muds, transported into the delta plain by a mixture of cyclones and constant tidal activity up the abandoned river channels, which post 5,000 yrs ago have been transformed into tidal-dominant estuaries.

The central criticism with these interpretations of lithofacies is that grain-size distributions (GSDs) represent a mixture of sediment populations, corresponding to different production and/or transport mechanisms (cf., Weltje and Prins, 2003; 2007). In the conceptual model of spatio-temporal grain-size variation developed by Weltje and Prins (2003; 2007), each size fraction corresponds to a characteristic process, termed a dynamic population (DP). DPs may be defined in probabilistic terms as an assemblage of grains that are likely to occur together, as they respond to dynamics of

sediment production and transport in a similar manner (Weltje and Prins, 2003). DPs provide a link between GSD variation and palaeoenvironmental reconstructions, as they can be coupled with the physical laws that govern sediment production and transport (Weltje and Prins, 2003). Tying this understanding of GSD and physical laws of production and transport of sediments, means that when a sediment is being eroded, the probability of any grain going into transport increases with diminishing grain-size (McLaren and Bowles, 1985). Here we present the first discussion of the production and transport of sediment within the G-B Delta that more fully encompasses the various processes contributing to grain-size variability in TMF lithofacies. For the purposes of this study, analysis is focussed primarily on the TMF unit as described by Goodbred and Kuehl (2000a).

2.3. Mineralogy and geochemistry of the Ganges-Brahmaputra Rivers

Both the Ganges and Brahmaputra rivers drain lithologically complex basins and lack a dominant lithology (Small et al., 2009). The drainage basin of the Ganges River is composed of highly weathered sediments and volcanics with clay dominance (Coleman, 1969; Lupker et al., 2012; 2013; Goodbred et al., 2014). Detrital grains of higher quartz and lower feldspars contents in surface sediments of the Bengal Basin (BB) are indicative of a source zone of low-relief tropical weathering (Potter, 1978; Datta and Subramanian, 1997). The lack of BB carbonate minerals is attributed to both weathering and the settling effects of detrital carbonates during transport in the upper reaches of the G-B Rivers (Datta and Subramanian, 1997).

The Ganges catchment streams draining the Himalaya have been well studied (e.g., Galy and France-Lanord, 1999; Dalai et al., 2002; Bickle et al., 2003, Chakrapani, 2005; Garzanti et al., 2010, 2011; Fontorbe et al., 2013; Frings et al.

2015) and are characterised by sediment supply from rapid physical and chemical weathering. Carbonate weathering is dominant with minor contributions from silicate weathering and hot springs (Frings et al., 2015). Differences in chemistries of headwaters in the southern tributaries of the Ganges compared to other streams draining the Himalaya have found cation compositions dominated by Na^+ (Rengarajan et al., 2009) instead of Ca^{2+} (Frings et al., 2015).

Detrital micas dominate the clay fraction (~80%) in Himalayan streams of the Ganges with authigenic clays more dominant in the alluvial plain (Chakrapani et al., 1995). The alluvial plain is the dominant zone of weathering and clay formation in the G-B Rivers with predominance of illite and kaolinite (Sarin et al., 1989; Chakrapani et al., 1995; Datta and Subramanian, 1997; Heroy et al., 2003; Frings et al., 2015).

The key distinction between the Ganges and Brahmaputra is silica enrichment in the sand fraction of Ganges sediment—attributable to chemical weathering of feldspar (Singh et al., 2005a, b; Bhuiyan et al., 2011). Fluvial transport is considered a major source of mineral sorting, controlling the geochemistry of weathering products (Singh et al., 2005a). Sediments in the upper catchment of the Ganges, the Ganges Alluvial Plain (GAP), have undergone chemical weathering of incipient to moderate intensity, with a first-stage of weathering in the Himalayas, followed by a second stage of weathering in the GAP (Singh et al. (2005a). The clay mineralogy and chemical index of alteration (CIA) (Nesbitt and Young, 1982) of sediments in the Brahmaputra show that weathering is generally less intense than in the Ganges and GAP (Singh et al., 2005b; Bhuiyan et al., 2011). This lower weathering intensity is attributed to higher runoff rates with greater physical erosion within the Brahmaputra. Heavy rainfall occurs during the SW and NE monsoons in the eastern

Himalaya and, as a result, there is increased runoff, which limits the potential for alteration of sediments through chemical weathering (Singh et al., 2005b).

Rogers et al. (2013) examined present-day sediment composition through sediment traps and radioisotope geochemistry, particularly through inventories of ^{7}Be ($t_{1/2}$ = 53.3 days; 477.7 KeV), ^{210}Pb ($t_{1/2}$ = 22.3 years; 46.5 KeV), ^{234}Th ($t_{1/2}$ = 24.1 days; 63.3 KeV) and ^{137}Cs ($t_{1/2}$ = 30.1 years; 661 KeV). The results from the inventory of ^{7}Be have shown that atmospheric deposition cannot alone be responsible for accumulation of ^{7}Be in sediments (Rogers et al., 2013). It has been proposed that ^{7}Be can only be added with the input of new sediment (Rogers et al., 2013). These findings from Rogers et al. (2013) indicate that there is rapid transport of G-B sediments to the inner BB shelf, sourced from sediment eroded from the surface of the G–B fluvial catchment. While on the coastal shelf, the river sediment plume is dispersed westward by prevailing currents. This sediment plume remains in suspension and available for transport onshore through a series of tidal creeks and onto the subaerial delta plain (Kuehl et al., 1989; Barua et al., 1994; Rogers et al., 2013).

In a previous study, Flood et al. (2016), the joint geochemical and grain size composition from the West Bengal Sundarbans was modelled using compositional data analysis (CoDa) and partial least squares (PLS) regression. It was found that there was a strong relationship between zirconium (Zr) and coarse grained sediment, with coarse clay and medium/coarse-silt found to be related to rubidium (Rb). Fine-grained sediment provenance was found to relate to Rb and K, with coarse grained sediment provenance linked to Zr. Calcium was interpreted to relate to external environmental controls (e.g., sea-level/ tidal inundation) as Ca is generally only present in liquid form in the marine environment. There was a negative covariance of

Ca with Zr, Ti, K, and Rb with decline in Ca and concomitant increases in Zr, Ti, K, and Rb interpreted as terrestrial derived sediment flux with diminished marine or carbonate deposition (Flood et al., 2016).

3. METHODOLOGY

3.1. Fieldwork

Coring was carried out using a motor driven percussion coring device with latitude, longitude and elevation recorded with a differential GPS and reported as above mean sea-level (amsl). Coring was carried out at Lothian (21° 42' 0.9252" N, 88° 18' 46.0188" E; 4.539 amsl), Gplot (21° 41' 24.3456" N, 88° 24' 9.4788" E; 2.532 amsl), and Dhanchi (21° 41' 57.7536" N, 88° 26' 1.896" E; 5.894 amsl) in November 2010 (sites shown in Fig. 1(ii)). These cores were all taken through the TMF sequence, varying between 5-7 m overall depth, before moving into the underlying sand facies of the fluviatile dominated delta. In total, 202 samples (8 cm apart) were collected from the three cores (Lothian, n=83, Gplot, n=46, and Dhanchi, n=73). Samples were divided into three groups for laboratory analysis (i.e., laser granulometry, XRD, and XRF).

3.2. Analysis of grain-size distributions

GSDs were analysed following Flood et al. (2015; 2016) using a MalvernMastersizer 2000 instrument. Data were aggregated into quarter phi intervals (φ scale) over the range of 0.02 – 2000 μm. Analysis of GSD composition followed the methodology developed recently by Flood et al. (2015) through compositional data analysis (CoDa) and multivariate statistics through principal components analysis (PCA) and cluster analyses (CA). In order to assess the textural characteristics of sediments from the Sundarbans, this study has adopted the approaches advocated by Flood et al.

(2015), whereby the GSD data are log-ratio transformed. A description of these statistical procedures are outlined in Flood et al. (2015; 2016). PCA and CA results from Lothian Island GSDs have been published previously (Flood et al., 2015) and will not be presented again in this study.

Centred log-ratio (clr) transformation was carried out on the GSDs prior to multivariate statistical analysis using the 'compositions' package for the R statistical environment (R Development Core Team, 2011). R was downloaded freely at http://www.r-project.org for Windows (current version 3.4.1, ~ 62 MB). PCA, hierarchical cluster and k-means cluster analyses were carried out on the log-transformed GSDs using the statistical package IBM® SPSS® Statistics version 19.0.

3.3. X-ray diffraction and mineralogical analysis

Selected core samples were lightly homogenised to an equal grain size fraction (<75 μm fraction) using an agate mortar and pestle in order to determine sediment mineralogy. X-ray powder diffraction (XRPD) was performed using a 3 kW PANalytical X'pert Pro Powder Diffractometer (Almelo, The Netherlands) θ/θ goniometer with a $CuK_{\alpha 1}$ electrode producing monochromatic radiation (λ = 1.54060 Å, 40 kV, 40 mA) between 3 and 63°2θ with a step size of 0.02° using an X'Celerator multichannel detector.

Qualitative and quantitative analyses of XRD data was performed using X'Pert HighScore Plus software, Version 2.2b (2006) with mineral identification performed with the JCPDS PDF-2 database from the International Centre for Diffraction Data® (ICDD, 2002). Multivariate statistical methods were employed to detect, describe, and classify patterns within the mineralogical data. PCA and

hierarchical cluster analysis (HCA) was carried out to allow samples to be agglomerated into representative mineralogical groups.

The Rietveld refinement method (Rietveld, 1967; 1969) of quantitative analysis was performed on diffraction samples originating from the cluster centroids most representative of the cluster groups. The Rietveld refinement method involves fitting an observed diffraction pattern with a synthetic pattern, which is a sum of patterns calculated for each phase in the sample (Snyder and Bish, 1989; Bish, 1994; Hillier, 2000). XRD was repeated on the cluster representative samples (between 3 and 65° 2θ with a step size of 0.02°) with further qualitative analysis. The output parameters from the fitting procedure are presented as a set of agreement indices following the refinement.

3.4. X-ray fluorescence and geochemistry

Data acquisition using ED-XRF was undertaken following the approach outlined by Flood et al. (2016), using a Bruker S1 TURBO SD portable X-ray fluorescence (PXRF) spectrometer (Bruker Corporation, Massachusetts, USA) consisting of a 10 mm X-Flash® SDD Peltier-cooled detector with a 4-W X-ray tube with an Ag target and a maximum voltage of 40 kV. Analysis was performed on discrete samples collected from the Lothian, Gplot, and Dhanchi Island cores. These samples were each measured for 30 seconds, with a set of 22 international geochemical reference standards (see supplementary appendix) measured for 120 s, this was performed for instrument calibration purposes. The 10 elements that are generally listed as oxides in the major element chemical analysis, Al, Si, Ti, Fe, Mn, Mg, Ca, Na, K, and P were determined in all samples. Trace elements Ba, V, Cr, Co, Ni, Cu, Zn, Rb, and Zr were also analysed. The precision and accuracy of the preparation and the

instrumental performance of the PXRF was checked using the international reference samples and a summary of these is provided by Flood et al. (2016). No discrepancies were found between the analytical data obtained and the consensus data with the international reference samples.

3.5. Major and trace element interpretation

Sundarban sediment maturity classification was obtained using, the Na_2O/K_2O ratio index of chemical maturity (Pettijohn et al., 1972), and the Fe_2O_3/Al_2O_3 ratio for mineral stability (Herron, 1988). These were plotted against SiO_2/Al_2O_3 ratio as an assessment of quartz and clay mineral abundance (Potter, 1978). A bivariate plot of major element geochemistry has also been used to infer tectonic provenance, using K_2O/Na_2O plotted against SiO_2 (Roser and Korsch, 1986).

In order to quantify weathering intensity the use of the CIA as proposed by Nesbitt and Young (1982) was applied in this study, where:

$$CIA = [Al_2O_3/(Al_2O_3 + CaO^* + Na_2O + K_2O)] * 100 \quad \text{Eq. 1.}$$

Taking the molecular proportions, and with CaO^* representing CaO in silicates only (Nesbitt and Young, 1989; Nesbitt et al., 1996). In this approach, a CIA value of 100 would suggest intense chemical weathering along with complete removal of all the alkali and alkaline earth elements (Singh et al., 2005a). CIA values of 45–55 indicate almost no weathering (Singh et al., 2005a). CIA values for average upper continental crust (UCC) and unaltered granite rocks are at 47 and 50, respectively (Singh et al., 2005a). A correction for CaO is required in order to account for the presence of Ca in carbonates and phosphates and this is generally conducted by calculating corrections

from measured CO_2 and P_2O_5 contents (Singh et al., 2005a). Where these data are unavailable, approximate corrections can be made by assuming reasonable Ca/Na ratios in silicate material (Singh et al., 2005a). In this study, CaO content was corrected for phosphate using available P_2O_5, where if the remaining number of moles is less than that of Na_2O, this CaO value was adopted (cf., Singh et al., 2005a). The rationale for using CIA is that it offers a quantitative measure of feldspar weathering by relating Al, which is enriched in the weathering residues, to Na, Ca, and K, which in principal should be removed during plagioclase and K-feldspar weathering (Nesbitt and Young, 1982; Sheldon and Tabor, 2009; Buggle et al., 2011). As clay content increases there should also be an increase in Al, whereas Ca, K, and Na should decrease, leading to higher CIA values (Sheldon and Tabor, 2009).

The identification and evaluation of major element mobility within the Sundarbans during weathering was carried out using elemental ratios calculated with respect to the least mobile element Al, which is believed to stay in the weathered material (cf., Singh et al., 2005a). The ratio of the content of element $\boldsymbol{D}$ and Al_2O_3 in the Sundarbans sediments was divided by the ratio of the same element content in UCC in the following element ratio:

$$Element\ ratio\ (\boldsymbol{D}) = \frac{\boldsymbol{D}/_{Al_2O_3(Sundarbans\ sediments)}}{\boldsymbol{D}/_{Al_2O_3(UCC)}} \qquad \text{Eq. 2.}$$

This ratio refers to the relative enrichment or depletion of the element with a value of >1 indicating enrichment, <1 indicating depletion, and = 1, indicating no change in the relative abundance.

As weathering proceeds, the mobilisation, fractionation, and redistribution of major and trace elements takes place, and as a result, weathering is impacted by dissolution and formation of primary minerals and secondary minerals, respectively

(Chesworth et al., 1981; Nesbitt et al., 1980; Fritz and Mohr, 1984). Along with these, redox processes, transportation, co-precipitation and ion exchange with various minerals may take place (Chesworth et al., 1981; Nesbitt et al., 1980; Fritz and Mohr, 1984). Since titanium is a relatively immobile element during weathering (Nesbitt, 1979), it has been used previously by Singh et al. (2005a) for the calculation of chemical mobility of major and trace elements. Following this approach, the percentage increase and decrease of a selected element, element ***D***, was calculated in the following manner:

$$Percentage\ change\ (\%) = \left\{\left(\boldsymbol{D}/_{TiO_2}\right)_{sample}/\left(\boldsymbol{D}/_{TiO_2}\right)_{UCC} - 1\right\} \qquad \text{Eq. 3.}$$

Relative to TiO_2, percentage change of elements were plotted against the CIA and provide a basis for assessing the increase or decrease in chemical mobility during chemical weathering (cf., Singh et al., 2005a).

These data are examined with reference to published data from Singh et al. (2005a) and Bhuiyan et al. (2011), for the GAP in India, and Brahmaputra–Jamuna River in Bangladesh, respectively. Data for UCC from Taylor and McLennan (1985) and World Sediments from McLennan (1995) are discussed to facilitate interpretation of the data from this study, alongside Singh et al. (2005a) and Bhuiyan et al. (2011).

4. RESULTS

4.1. Multivariate statistical analysis results from Gplot and Dhanchi grain-size distributions: PCA and CA results

Figure 2 (a-c) shows the percentage (%) sand, silt, and clay composition from the Lothian, Gplot, and Dhanchi Island cores, respectively. The overarching grain size is silt which comprises ~70 – 80% of the sediment, with Gplot showing a proportionally higher sand content.

The results from the multivariate statistical analysis of GSDs from the Gplot and Dhanchi Island cores are shown in Fig. 3(a-j). Coefficients from the first and second principal components (PCs) from Gplot are shown in Fig. 3(a, b) with PC1 (Fig. 3a) illustrating very coarse silt to fine-medium sand (4.00 φ–1.25 φ) and negative coefficients corresponding to fine clay to coarse silt fractions (12.02 φ–4.24 φ). PC2 coefficients (Fig. 3b) show highest positive values for coarse silt and very coarse silt, with highest negative values for fine and medium sand. Table 1 summarises the PCA carried out from the first four PCs (~95% of variance), with 71% of the cumulative variance of PC1 and 14% by PC2.

Vertical distribution of PC scores for Gplot are shown in Fig. 3(c, d) with PC1 (Fig. 3c) scores showing positive scores from the base of the core, at ~ 386 cm to a depth of ~ 230 cm. Positive scores from ~ 230 cm progress into negative scores up to the core surface. This succession is interpreted as dominant fining-up in the core, with coarse material (sand and coarse silt) dominant at the core base, then, at ~ 200 cm, the position is reversed with the predominance of medium – fine silt and clay and the absence of sand and coarse silt.

PC2 scores (Fig. 3d) reflect that within this fining-up of the sequence, varying degrees of silt composition make up the core with some sandy and coarse material interspersed throughout with negative scores in PC2 reflecting very-coarse silt and sand.

Cluster analysis (CA) through Ward's (1963) hierarchical cluster analysis (HCA) and k-means cluster analysis indicate that three groups of sedimentary facies effectively explain the GSD variation, with their vertical disposition depicted in Fig. 4(a). The grain size association with each of the sedimentary facies follows:

- Facies 1a (F1a): medium clay to medium silt;
- Facies 2a (F2a): medium to very coarse silt with some sand, and;
- Facies 3a (F3a): composed of very fine to very coarse sand.

From the base of the core to a depth of 250 cm there are fluctuating trend between F3a and F2a. From 250 cm to 200 cm the cluster membership is mainly composed of F2a, with a fluctuating membership of F2a to F1a from 200 cm to 40 cm. From 40 cm to the core surface the sequence is primarily composed of fine-to-medium silt and clay. The fluctuating variability in cluster group association appear indicative of the PCA results, with F3a, and F2a composed of varying levels of sand and silt (coarse–medium) while F1a appears to be characteristic of fine and medium silt with clay composition. The vertical trend of these groups through the Gplot Island core indicates a fining-up sequence (Fig. 4(a)).

Association of these sedimentary facies to PCs extracted is illustrated in Fig. 3(e), with a biplot of PC1 and PC2. PC1 is interpreted as fining-up trend (horizontal axis) with PC2 of an oscillating trend between coarse and fine material. Sample points located in the positive quadrant for PC1 and 2 reflect very-coarse silt and fine sand composition that comprise F2a samples. Samples in the positive PC1 and negative PC2 quadrant reflect very-coarse silt with fine-medium-coarse sand with F3a samples in this quadrant indicative of sand near the core base. Samples in the negative PC1 and PC2 quadrant are composed of F1a, indicative of medium clay to fine silt in the upper parts of the core. A facies transition order is present, with

coarser sands and coarser silts at the core base, overlain by a greater oscillating pattern of cluster groups from ~ 200 cm to core surface (Fig. 4(a)). The ordering and appearance of sedimentary facies suggests there are two distinctive broad stratigraphical Facies; (i) a lower sandy-silt; and (ii) an upper oscillating sequence of fine/medium-silt and clay, as shown in Fig. 4(a).

Dhanchi grain-size coefficients from PC1 and PC2 are shown in Fig. 3(f,g) with positive coefficients from PC1 (Fig. 3f) corresponding to medium clay and very coarse silt (12.02 φ–6.00 φ) and negative coefficients for very coarse silt to sand fractions (5.01 φ– −1.00 φ). PC2 coefficients (Fig. 3g) indicate highest positive values are very coarse silt (5.00 φ–4.00 φ) and coarse silt (6.00 φ–5.00 φ), with high negative coefficients indicative of clay (7.00 φ–6.00 φ) and sand (4.00 φ– −1.00 φ). Table 2 is a summary of the PCA with the first four components (~99% of variance), with PC1 comprising ~ 86% of the cumulative variance and PC2 of 8% of cumulative variance.

Fig. 3(h, i) shows the score distributions throughout the Dhanchi core for PC1 and PC2. PC1 scores (Fig. 3h) show that from core base to ~ 300 cm depth, sediment is composed of very coarse silt and sand with some finer material (clay and fine silts) and overlain by coarser sediment from ~ 300 cm to the core surface. PC2 scores (Fig. 3i) show fluctuating coarse sediment throughout the core, with highest positive scores for coarse silt and sand with finer-grained sediment between ~ 450 cm to 0 cm, denoted by slightly negative to low scores. Results indicate that the sequence is composed almost entirely of various grades of silt with clay, and sand. These characteristics would suggest a mixture of size fractions throughout the Dhanchi sequence but with dominant fining-up.

HCA and k-means cluster analysis show three groups of sedimentary facies that explain GSD trend in the Dhanchi core (Fig. 4b). Grain size association with each of the sedimentary facies is:

- Facies 1b (F1b): two samples, considered to be an outlier;
- Facies 2b (F2b): two samples, considered to be an outlier;
- Facies 3b (F3b): medium and coarse silt with clay;
- Facies 4b (F4b): coarse silt with some sand, and;
- Facies 5b (F5b): sand (very fine sand to very coarse sand) with silt.

From core base to 320 cm a fluctuating trend between F5b and F4b is found, and from 320 cm to 60 cm cluster membership varies between F4b and F3b, with the top 60 cm composed of F3b and some F2b. F5b, F4b. F3b indicate varying degrees of silt (coarse–medium–fine) and sand, F4b and F3b comprising fine and medium silt with clay, with F1b of coarse silt, and F2b clay. Sand and silt fluctuations are shown by F5b and F4b, with F4b and F3b for coarse silt to medium and fine silt.

Biplot analysis of sedimentary facies and PCs from the Dhanchi are shown in Fig. 3j. Biplot quadrants reveal that in positive PC1 and PC2, there is an overall coarse-silt composition. Positive PC1 and negative PC2 reflect predominantly F4b samples with F4b samples most negatively represented along the second principal component, indicative of very-coarse silt to sand, with F5b showing the transition from very-coarse silt and sand to very-coarse clay and medium clay. The negative PC1 and PC2 quadrant is composed of some F4b and F5b samples, with negative PC1 and positive PC2 quadrant composed mainly of F5b and F1b.

PC1 is interpreted as a fining-up trend (horizontal axis) with PC2 composed of coarse-silt and sand fractions. Positions of some outliers in the F1b and F2b samples show the latter indicative of coarse- to very coarse-silt and former of sand

and clay. Cluster groups of F4b and F3b represent coarse sediment (coarse silt and sand), with F3b of the progression into fine material and fining-up. Facies order or stacking pattern is present, coarser silts and sand dominating the sequence from core base at 558 cm to ~ 250 cm, overlain by an oscillating trend of cluster groups ~ 250 cm to ~ 60 cm. The oscillating trend is overlain by homogeneous, medium- and finer-silts with clays from ~ 60 cm to core surface (Fig. 4b). Ordering of sedimentary facies and appearance in core suggests there are three distinctive broad stratigraphical facies; (i) a lower coarse-silt and sand; (ii) a middle medium-fine silty-clay; and (iii) an upper medium- to very fine-silt and clay.

4.2. X-ray powder diffraction: results from the Sundarbans

Table 3 shows the most representative cluster samples with their site and depth in each core with data analysis outlining mineral groups within the cores. Following Rietveld refinement, observed and calculated spectra for cluster representative samples are given in supplementary data. Agreement indices for each diffractogram are shown in Table 4 with 'goodness-of-fit' best interpreted from the residual (R_p) and weighted residual (R_{wp}) profiles. Optimum fit based on these parameters is generally less than 5% and 10% for R_p and R_{wp}, respectively. These are expected to be a little higher in geological material (O'Meara 2013, pers. comm.; Speakman 2013, pers. comm.; Pecharsky and Zavalij, 2009).

Cluster 2 appears to have refined optimally (R_p = 5.5% and R_{wp} = 7.6%), and cluster 4 having the highest residual values (R_p = 15.3% and R_{wp} = 25.0%) with clusters 1, 3, 5, and 6 having a series of residual and weighted residual values between 13.1–9.3% and 9.1–6.2%, respectively. Rietveld Refinement carried out on the six cluster representative samples appears to show well-fitted models for the

observed spectra. Mineralogical composition is shown in Table 5 with a data summary in Table 6.

High abundance of quartz is found in all clusters with cluster 4 and 2 having the highest (78.6%) and lowest (34.8%), respectively. Clinochlore was present in all but two clusters (2 and 5) with highest (5.5%) and lowest (0.9%) in 6 and 4, respectively. Muscovite was found in nearly all clusters, except cluster 4, with highest (50.9%) and lowest (18.8%) in cluster 2 and 1. Albite (plagioclase feldspar) present in all clusters with highest (13%) and lowest (4.9%) contents in cluster 5 and 4, respectively. Microcline (alkali feldspar) was present in cluster 4 at 8.2 %. Clay minerals consisted of kaolinite, dickite, and possibly vermiculite at only trace amounts (<1.0%) detected in clusters 2 and 5 at 0.7 % and 0.4 %, respectively. Dickite (polymorph of kaolinite) was present in cluster 4 (4.6 %), with kaolinite in all cluster representative samples, with the exception of cluster 4. The highest (13.6%) and lowest values (6.7%) of kaolinite were in cluster 2 and 5, respectively.

A plot of the first three principal components is shown in Fig. 5, with ~95% of the variance accounted by these components. PC1 is composed mainly of quartz in all of the samples examined (Table 5) with phyllosilicates, particularly mica (i.e., muscovite) and clays (i.e., clinochlore and kaolinite) illustrated by PC2. Feldspars (i.e., albite, microcline and Ca plagioclase) comprise PC3 with Fig. 5a showing cluster 5 in the negative PC1 and PC2 quadrant, potentially attributed to albite. Progression of scores along PC2 show predominantly clusters 3, 6, and 2, and reflect increasing muscovite and kaolinite composition (i.e., muscovite: 22.1% → 33.6% → 50.9%; kaolinite: 6.9% → 11.9% → 13.6%). This trend in PC2 appears to continue with cluster 4, with this cluster varying more positively in PC3, interpreted as high microcline content. Cluster 1 appears distinct as it tends to vary negatively along

PC2, reflecting lower quantities of phyllosilicates and having higher albite and clinochlore contents, with the latter absent from cluster 5.

The distribution of the mineral clusters from each of the Sundarbans cores is shown in Fig. 5(e), Lothian (i) displaying a sporadic and fluctuating trend in clusters 2, 4 and 6 at core base to c. 500 cm, and an oscillating trend between clusters 4 and 2 from c. 500 cm to c. 170 cm, overlain by another oscillating trend between cluster 5 and 3. Cluster 1 is dominant in Gplot core (ii) from the core base to c. 225 cm, followed by an oscillating trend between 6 and clusters 2 and 3 from c. 225 cm to core surface. Two oscillating trends are found in the Dhanchi core (iii), at the core base to c. 220 cm composed of clusters 2 and 4, followed by clusters 6 and 2 from c. 220 cm to c. 40 cm depth with a final oscillating trend from c. 110 cm to 50 cm with clusters 3 and 6.

4.3. X-ray fluorescence: results from major and trace element geochemistry of the Sundarbans

The bulk chemistry of the Lothian, Gplot, and Dhanchi island cores consists mainly of the oxides of three elements: Al, Si and, Fe. The total composition of these elements in Lothian, Gplot, and Dhanchi island cores is approximately 84%, 83% and 86%. The average SiO_2/Al_2O_3 ratios of Lothian, Gplot, and Dhanchi are 4.1, 4.5, and 4.2, respectively. This is interpreted to reflect mineral composition and grain-size variability, in which GSD is mainly silt-sized with quartz dominant in coarse-size fractions, and clay minerals in fine grain-size fractions. Aluminosilicate minerals are preferentially transported as suspended load with quartz tending to be found as bedload (cf., Singh et al., 2005a).

4.3.1. Rock classification and tectonic provenance of Sundarbans sediments

Ratios of the major elements of Al_2O_3/SiO_2 and Fe_2O_3/SiO_2 of the Sundarbans, along with data from Singh et al. (2005a) and Bhuiyan et al. (2011), were plotted with respect to the Himalaya and the Siwalik, following Singh et al. (2005a) (Fig. 6). The Himalayas tend to possess a mean chemical composition that is similar to the average UCC (Galy and France-Lanord, 2001). The linear relationship found with the Sundarbans sediments indicates a grain-size component, with the lower parts of each core being enriched with quartz. This is seen in Fig. 6 with the position of the Sundarbans samples from Lothian and Gplot being clustered in close proximity to the channel sediments samples from Singh et al. (2005a), with these samples understood to be enriched in quartz. This sort of mineral sorting response is further evidenced by the trend towards phyllosilicates that is substantiated by the presence of suspended sediments from Singh et al. (2005a). The Al_2O_3/SiO_2 and Fe_2O_3/SiO_2 ratios found in this study appear to reflect the compositional maturity of sediments, originating from the Himalayas and Siwaliks, and moving towards the delta, with the Sundarbans evidence of the highest weathering maturity.

The Pettijohn and Herron diagrams (Fig. 7a & b) indicate that clastic weathering products of the Sundarbans are primarily litharenite and greywacke/wacke, with Lothian and Dhanchi representing the most mature sediment. The presence of Gplot samples within arkose, with all Sundarbans samples plotting towards litharenite and greywacke/wacke, may be interpreted as grain-size variation with increasing clay content. The tectonic provenance discrimination plots show that the majority of the Sundarbans samples fall into the active continental margin field (Fig. 8), with some scatter of samples into the island arc field.

4.3.2. Element enrichment ratios for the Sundarbans

Element ratios in the Lothian, Gplot, Dhanchi, Singh et al. (2005a) and Bhuiyan et al. (2011) datasets are shown in Fig. 9. SiO_2 mobility is considered important for interpreting chemical weathering, soil formation and distribution of elements in natural waters (Singh et al., 2005a). There is a depletion in SiO_2 relative to Singh et al. (2005) data points, but enriched compared to Bhuiyan et al. (2011). Titanium is understood to be a relatively immobile element and appears to be most enriched in the Lothian and Dhanchi cores, but most depleted in the Gplot Island core. There is a progressive depletion in CaO and Na_2O throughout the Sundarbans cores, which is reflective of these being highly mobile elements. Potassium shows some depletion in the Sundarbans cores, with Gplot being more enriched in K_2O relative to Lothian and Dhanchi. As discussed by Singh et al. (2005a), potassium tends to be preferentially adsorbed to clay minerals, as found by Flood et al. (2016) for the Sundarbans. Therefore, the enrichment of K_2O may be due to silicate minerals formed during weathering or alteration of existing clay minerals such as montmorillonite, which tend to incorporate potassium relative to Na_2O (Singh et al., 2005a). Clay minerals also have a tendency to incorporate magnesium as well as K_2O, and lose Na_2O, which can be see with the pronounced enrichment of MgO in the Dhanchi and Lothian cores. Due to the highly mobile nature of Na_2O and CaO during weathering, these may be readily dissolved and taken up into and enriched in solution (i.e., in aqueous phase) as opposed to being deposited as part of the sediment load. This has been found by Singh et al. (2005a) and Singh et al. (2005b), who show a concentration of these elements in the dissolved fraction of fluvial sediments. MgO shows some mobility between sites in the Sundarbans with Lothian and Dhanchi

slightly enriched compared to Gplot. Although Mg may dissolve during weathering and enter the aqueous phase, it has been found to be depleted in channel sediments, but mobile within suspended and floodplain sediments (Singh et al., 2005a). This may explain the Mg variability between sites in the Sundarbans, with Gplot composed of coarse-grained, channel-type sediment, relative to Lothian and Dhanchi.

4.3.3. Inter-element variability from the Sundarbans

Fig. 10 displays inter-element relationships plotted on variation diagrams using Al_2O_3, SiO_2 and TiO_2 along the x-axis. In the majority of the variation diagrams, some linear trend from Lothian, Gplot, and Dhanchi are observed with positive or negative correlations. Relatively strong negative correlation of SiO_2 with Al_2O_3 and Fe_2O_3 indicates grainsize control on the geochemistry of the Sundarbans' weathering products, with little correlation (R^2 = 0.04) with K_2O. The increasing trend of TiO_2 with Fe_2O_3 is attributed to the enrichment of heavy minerals in Sundarbans sediments. However, MgO and K_2O have different patterns with Al_2O_3 and TiO_2, respectively. Plotting the chemically immobile TiO_2 against Al_2O_3 provides further insight into the hydrodynamic and chemical behaviour of the major mineral phases and indicates that they were concentrated into the fine-grained sediment fraction (i.e., monotonic relationship reflects decreasing grain-size). High concentrations of TiO_2 in Sundarbans sediments and a strong correlation with Al_2O_3 indicate that TiO_2 could potentially be derived from mica, although there is a poor correlation with K_2O and TiO_2. TiO_2 plotted against Fe_2O_3 displays a good correlation (R^2 = 0.68) indicating their common sources from ferromagnesium minerals such as biotite, amphibole, and pyroxene (cf., Singh et al., 2005a). A poor correlation of K_2O with MgO and Al_2O_3 indicates an absence (or failure to detect) of illite in these sediments (cf., Singh et al.,

2005a). The strong correlation found for Fe_2O_3 with Al_2O_3 may be associated with alteration of biotite into aluminosilicates and Fe(III) oxides (cf., Singh et al., 2005a). The distribution of major elements in the Sundarbans sediments suggests that weathering products have strong inter-elemental linkage.

4.3.4. A–CN–K diagram and chemical index of alteration (CIA) for Sundarbans

Fig. 11 (a) shows a ternary A–CN–K diagram along with the location of important rock-forming minerals, UCC (Taylor and McLennan, 1985) and natural waters (cf., Singh et al., 2005a). The sediments from the Sundarbans tend to plot towards the Al_2O_3 apex, indicating loss of Na and Ca during weathering compared to the UCC, with a tendency for samples to plot towards A–CN, with a slightly larger proportion of samples towards the A of the apex. CIA values for Lothian, Gplot, and Dhanchi are 46–67, 53–76, and 52–65, respectively. The average CIA of the Sundarbans is compared with Singh et al. (2005a) and Bhuiyan et al. (2011) (Fig. 11b). There appears to be a fair degree of weathering found in the Sundarbans sediments, with Gplot Island showing the highest mean CIA. The Sundarbans data show a higher degree of weathering, relative to Bhuiyan et al. (2011) from the Brahmaputra-Jamuna River. With the exception of the flood and suspended sediment CIA values of Singh et al. (2005a), the Sundarbans CIA values show an increasing degree of weathering compared with channel sediments.

4.3.5. A–CNK–FM and S/10–CM–NK variability of the Sundarbans

Shown in Fig. (12 c,d) are A–CNK–FM and S/10–CM–NK ternary plots (Nesbitt and Young, 1989; Singh et al., 2005a). Sundarbans samples tend to be positioned in the centre of the ternary diagram (Fig. 11c), with Gplot closer to feldspar composition

(cf., Singh et al., 2005a). Increased weathering of fine-grained material, tends to have a winnowing effect of Fe-oxyhydroxides and biotite, which may explain the enrichment towards the FM apex with Lothian and Dhanchi (cf., Singh et al., 2005a). The presence of suspended sediments from Singh et al. (2005a) closest to the FM apex may indicate secondary sedimentary processes concentrating heavy minerals in sediment (Singh et al., 2005a). The suspended sediments from Singh et al. (2005a) may be considered to be one end-member in this ternary diagram, with Gplot being the opposing end-member in the A–CNK apex. The arrows depicted show the predicted weathering trends that have been found in the GAP, in which Sundarbans samples appear to following this predicted weathering trend.

In the S/10–CM–NK diagram (Fig. 11d) all of the Sundarbans samples plot away from the S/10–CM apex and towards NK, with Gplot samples plotting more strongly towards the S/10–NK apex and, Lothian and Dhanchi plotting towards the CM-NK apex. Compared with Singh et al. (2005a) and Bhuiyan et al. (2011), there is some similarity present, with the exception of suspended sediments of Singh et al. (2005a) which plot towards the CM apex. The position of the Gplot samples at the S/10–NK apex may be attributed to greater quartz presence in these samples, relative to Lothian and Dhanchi, which show a decrease in quartz, as these plot towards the CM–NK apex.

4.3.6. Chemical mobility within the Sundarbans Holocene sediments

The chemical mobility is shown in Fig. 12 for the Sundarbans sediments during weathering processes, and is calculated in terms of % change normalised to TiO_2 for individual major/trace elements against progressive chemical alteration, using the CIA values. A decreasing trend was found in chemical mobility of Na_2O_3 (a), MgO

(b), Al_2O_3 (c), SiO_2 (d), K_2O (f) in all cores, with CaO (g) and Zr (q) showing the greatest decreasing trend. An increase was found in P_2O_5 (e) and Fe_2O_3 (i) mobility, with an unvarying trend in Ba (j), and V (k). Mn (h), Cr (l), Ni (m), and Cu (n) appear to have no discernible trend with CIA. A slight increase was found in Zn (o) with a slightly greater increase in Rb (p) with increased CIA.

5. DISCUSSION

Deposition of the TMF in the far western extent of the Sundarbans is shown in Fig. 13. There is a gradual shift in the dominance of fluvial processes in deposition from c. 5,000 cal yr BP to a more mixed fluvio-tidal depositional system from c. 3,000 cal yr BP, to its current state as a tidal dominant delta. Sedimentation rates for the present-day eastern Sundarbans have been reported as being c. 1.0 ± 0.9 cm yr^{-1} (Rogers et al., 2013) whereas Flood (2014) and Flood et al. (2015) determine a sedimentation rate of c. 1.4 mm yr^{-1} for the far western Sundarbans over the late Holocene (c. last 4,000 cal yrs). The model proposed in this study is that there is a gradual (or rapid) loss of the westerly tidal transported sediment plume along the Bay of Bengal coastline. This primarily suspended load then moves up the flood dominant estuaries of the Sundarban blind rivers (Bhattacharyya et al., 2013), to be deposited in the distributive system between estuaries, as the sediment plume moves westward (cf., Rogers et al., 2013). The TMF in the most western extent of the G-B delta is proposed as being a diachronous facies unit, with fluvial dominance prevalent c. 5,000 yrs BP that gradually developed into a mixed fluvio-tidal dominant delta from c. 3,000 yrs BP, to being a tidal dominant delta at present. Sediment is sourced primarily from the Ganges river and delivered to the coastal shelf as a plume that is re-worked onto the delta plain with the emerging tidal

supplied sediment plume thinning in volume and sediment size as it is carried further west to the tidal dominant delta (Fig. 13). The depositional model proposed in this study is a series of incremental developments from previous studies, particularly from Goodbred and Kuehl (2000a), Allison et al. (2003), and Rogers et al. (2013). The TMF in the far western extent of the Sundarbans is considered to reflect abandoned floodplain overbank deposits (cf., Goodbred and Kuehl, 2000a). The processes of deposition reflecting tidal/marine processes (cf. Allison et al., 2003), with the source of the TMF sediments being the Ganges River associated with monsoon flood discharge and sediment being dispersed westwards by currents followed by onshore transport (Rogers et al., 2013).

5.1. Lithofacies variability and dynamics in the TMF: evidence from the West Bengal Sundarbans

The Lothian and Dhanchi Island GSDs may be interpreted as reflecting a muddy tidal flat environment with the overarching presence of silt and clay (e.g., Fig. 2, Fig. 4b), although it is difficult to determine sedimentary structures from the cores (cf., Allison et al., 2003; Goodbred and Saito, 2011; Flood, 2014; Flood et al., 2015).

The dominant upward-fining in GSDs from these cores may be attributed to slack water deposits as a result of tidal deposition (cf. Bass et al., 2002). In terms of silt and clay deposition through tides, suspension of sediments lasts longer than sands and may therefore be transported over long distances and may be advected into or away from a depositional site (Bass et al., 2002). These fining-up sequences, comprising muddy tidal flats may cap subtidal sand ridges (Wells, 1995). A similar model of facies succession has been proposed by Goodbred and Saito (2011), where

the migration of tidal channels and creeks across tidal flats, contribute to fining up facies succession. The clay fraction indicated by the first and second principal components may represent the mud-drapes and fluid-muds attributed to slack water or poor water flows (cf., Wells, 1995). However, this is difficult to judge as a limited sample population was used in the GSD analysis, thus only the general trend of fining-up (e.g., Dhanchi PCA score plots and GSD facies shown in Fig. 3(h, i)).

Gplot GSDs may be interpreted as sub- to intertidal-tidal flat environment (cf., Goodbred and Saito, 2011). Transition between the two broader sedimentary sub-units indicates the lower sub-unit was within closer proximity to fluvial sources of sediment given coarse GSDs (Fig. 2 and Fig. 3(a-d)) (Hughes, 2011). GSD interpretation indicates a correlation with effective transport energy as opposed to any direct correlation with proximity to marine or fluvial sources. With a relatively coarser sediment load, the probability of sediment transport processes that maintain such a sediment load decreases (McLaren and Bowles, 1985). As sediment deposits become coarser in a sequence, depositional processes take on the attributes of low-energy functions with sediments becoming finer (McLaren and Bowles, 1985). From Gplot, although coarse sediment is present, the likelihood of transitioning into a finer facies increases with time. Cross phase similarity with PC1 from Dhanchi and Gplot Island is found with signs being different – but PCs measuring the same phenomenon; dominant GSDs (Fig. 3 and 4). There is a similar fining-upwards drift through the core (Fig. 2 and Fig. 3(c-e)) with PC2 indicative of the presence or absence of the 4.5 to 7 φ elements, and acting as a bridge to the presence of very fine and slightly coarser sediment. Three broader stratigraphic facies have been identified in the Lothian and Dhanchi Island core data which are similar to those developed by Allison et al. (2003). It is proposed that the statistically derived facies presented in

this study may be considered to range over two of the principal facies that Allison et al. (2003) outlined in their study (i.e., those of the 'intertidal shoal' and 'supratidal' facies).

Lithofacies of the Sundarbans and the TMF demonstrate a high degree of variability between core-sites, however application of multivariate statistics offers enhanced scope for palaeoenvironment interpretation. The lithofacies models developed are applied to each site separately, with this approach taken given the GSDs from the Gplot Island core would skew the analysis of the GSD data from the Lothian and Dhanchi Island cores. Although the sites are relatively close (within 10 km), sediment dynamics and variability can be understood to be highly divergent when the Gplot GSD data is examined. One potential explanation for this variability may be in the depositional environment of the Gplot site. Tidal dominated environments are indicative of intertidal to shallow subtidal zones, which are dominated by muddy tidal flats and tidal channels and, may also include channel-mouth and channel-side bar features (Goodbred and Saito, 2011). These tidal ridges are understood to accrete vertically and horizontally (akin to subdued flooding levees, i.e., channel-side features) until forming a shallow intertidal flat with vegetation succession taking place (Goodbred and Saito, 2011).

5.2. Mineralogy of the West Bengal Sundarbans

Mineralogy from the West Bengal Sundarbans reveals key variability between the islands. Terrigenous minerals are abundant in all cores, principally quartz, feldspars, and muscovite mica. Quartz in Holocene sedimentary environments varies under a number of circumstances (see Wedepohl, 1978; Kabata-Pendias, 2001; Hinman, 1998; Salminen et al., 2005; Garzanti et al., 2011). Quartz in these sediments may

reflect detrital deposition of weathering-resistant sediment in the West Bengal Sundarbans. The Ganges River is understood to carry more quartz and less Ca-plagioclase than the Brahmaputra river (Garzanti et al., 2011). With increased erosion and sorting, the ratio of feldspar to quartz is generally diminished in sand composition with higher proportion of quartz indicative of coarse grain-size sediments (Nesbitt et al., 1996). This is seen in the mineral clusters 5, 4, 3, and 1 with mineralogy from Gplot (depth of c. 386 cm to c. 225 cm), having high quartz, muscovite, albite, and kaolinite contents.

There is a dominant fluctuation between high quartz and high muscovite in Dhanchi, particularly in clusters 2, 4, and 6 (core base to c. 220 cm). Mica may illustrate winnowing and active deposition on continental shelf systems (Doyle et al., 1968; Adegoke and Stanley, 1972; Doyle et al., 1979; Dias et al., 1984). Common minerals like quartz, feldspars, and calcite are generally associated with significantly reduced heavy mineral loads (Garzanti et al., 2008). Heavy minerals tend to be enriched in the fine tail of the grain size distribution with quartz, feldspars, and calcite found to comprise the coarse tail (Garzanti et al., 2008). Thus, micas make up the coarsest tail of a grain size distribution for sediment due to their platy shape, with the finest grain size fraction composed of zircon, monazite or magnetite because of their extreme density (Garzanti et al., 2008). The predominance of mica and reduced quartz content from the base of the core to c. 220 cm reflect this variability in hydrodynamic sorting of minerals. From 220 cm to the core surface, mica composition is reduced with much less variability in quartz composition (see Table 5 and Fig. 5).

In the Lothian core, fluctuations between clusters 2, 4, and 6 from the base of the core to c. 500 cm may reflect variability in sand and silt deposition. Cluster 2 has

higher muscovite abundance (50.9%) relative to quartz (34.8%) with cluster 4 made up of 78.6% quartz and no muscovite, variability in these detrital minerals may be a result of diverging settling velocities (cf., Dias et al., 1984). Mineralogical variability over time scales of centuries of deposition in terms of sediment hydraulics may be attributed to the relative height of the tidal frame and the upward development of an intertidal mudflat (cf., Allen, 1990; 2000), with fluctuations in tidal frame that contribute fluctuations in settling of finer (i.e., muscovite) with coarser sediments (i.e., quartz grains). Cluster 6 is composed of nearly equal quantities of quartz and muscovite at 38.8% and 33.6%, with kaolinite at 11.9%, indicative of reduced energy.

Chemical weathering in lowland rivers may control the formation of kaolinite from feldspars and mica mineral assemblages, demonstrated in Fig. 14(a) where a strong correlation is found between muscovite and kaolinite. Smectite, attributed to be an indicator mineral for Ganges sediment provenance (Heroy et al., 2003) was not found in this study or by Sarin et al. (1989), where kaolinite content ranged between 6.7% and 13.6%. The lack of smectite is attributed to the requirement of dehydration experiments needed for positive smectite identification. Illite was not found either but may be attributed to late stage weathering within the GAP (cf., Singh et al., 2005a).

Kaolinite and muscovite percentages shown in Fig. 14(a) (R^2 = 0.90), show kaolinite formation possibly a function of weathering in mica (cf., Stoch and Sikora, 1976). Muscovite mica to kaolinite formation is the result of transformation of: muscovite → mixed layer muscovite/montmorillonite → montmorillonite → kaolinite (Stoch and Sikora, 1976). It is uncommon for montmorillonite to be found

and this may be due to montmorillonite existing in an unstable intermediate phase during weathering (Stoch and Sikora, 1976).

Kaolinite and quartz shown in Fig. 14(b) being highly negatively correlated (R^2 = –0.96). Correlation is attributed to grain-size variability and has been known to occur in estuaries where quartz is dominant in sand and phyllosilicates in greater abundance in finest fraction (Galán et al., 2003). Where there are greater quantities of quartz there is a concomitant decrease in kaolinite.

Oscillating trends in mineral clusters found in the Dhanchi core are indicative of silt and sand-size sediment, similar to the Lothian Island core, with the Gplot core showing oscillating variability in mineral clusters associated with high mica and quartz content, indicative of varying deposition in sand and silt. As the feldspar is composed mainly of albite, chemical weathering tends to alter plagioclase feldspar as opposed to K-feldspar and quartz, with the abundance of albite indicative of weathered sediment (Grant 1963; Nesbitt and Young 1989; Nesbitt et al., 1996).

High quartz content compared to other minerals is indicative of low-relief tropical weathering within the Bengal Basin (Potter, 1978; Mukherjee et al., 2009). In gentle slopes, water easily penetrates into the substrate, dissolving the most soluble constituents and accumulating the less mobile ones (Gutierrez, 2005). Formation of kaolinite from feldspar and mica in soil and sediments as a result of meteoric water drainage (Islam et al., 2002; Bjørlykke, 1998). This has been known to occur within warm, humid climates, particularly under tropical conditions (Islam et al., 2002). Formation of kaolinite is due to greater leaching conditions with high-rainfall (Ehlmann, 1968; Islam et al., 2002).

5.3. Geochemistry of the West Bengal Sundarbans

The geochemistry of the Holocene sediment from the West Bengal Sundarbans can be characterised as intensively weathered, terrestrial sediment derived from the Ganges River, principally the GAP. Therefore we suggest that sediments of the TMF are derived from the weathering and transport of Himalayan derived sediments, with geochemical data supporting the two stage weathering model proposed by Singh et al. (2005a), with initial weathering in the Himalaya and subsequent weathering under a humid sub-tropical climate (Singh et al., 2005a). The first and second weathering cycles are related to illite, and smectite dominance, respectively (Sarin et al., 1989; Singh et al., 2005a). Although illite-smectite variability was not found in this study, several aspects of the geochemical data validate both the source and processes (i.e., 'second cycle' weathering products) in the TMF of the West Bengal Sundarbans.

The maturity of sediments in the Sundarbans can be derived from Fig. 6 and from Fig. 7(a) following the Pettijohn et al. (1972) index of chemical maturity with mineral stability following Herron (1988) (Fig. 7b). The Al_2O_3/SiO_2 versus Fe_2O_3/SiO_2 presented in Fig. 6 for the Sundarbans along with the Siwaliks and the Himalayan sources show that the increasing ratios from low-to-high are indicative of decreasing quartz proportion and enrichment in phyllosilicates, respectively (Singh et al., 2005a; Garzanti et al., 2010; Garzanti et al., 2011). The linear trend shown in Fig. 6 may correspond to mineralogical sorting of sediments during transportation (Singh et al., 2005a; Garzanti et al., 2008; Garzanti et al., 2009). The lower ratios found in samples from Gplot, with the subsequent increasing trend, indicate increasing compositional maturity in Sundarbans sediments (cf., Singh et al., 2005). Textural maturity is further substantiated by the Pettijohn et al. (1972) classification scheme, where the majority of Sundarbans samples are found to be mostly litharenite and

greywacke/wacke. Mineral stability in the modified classification scheme of Pettijohn et al. (1972) by Herron (1988) shows a consistency in the Sundarbans being mineralogical mature, with most samples found to be litharenites and wacke (Fig. 7b). As discussed by Herron (1988), the Fe_2O_3/K_2O ratio can be considered an indicator of mineralogical stability. The most stable rock-forming minerals found at low temperature and pressures in sedimentary environments are K-feldspar, muscovite mica, and quartz (Herron, 1988). K-feldspar and muscovite mica tend to have high quantities of K, and in all three there is a low Fe content (Herron, 1988). There tends to be a higher Fe and Mg content in less stable rock-forming minerals (Herron, 1988). Stable mineral assemblages therefore possess low Fe_2O_3/K_2O ratios, while less stable mineral assemblages that are found close to sediment source have high Fe_2O_3/K_2O ratios (Herron, 1988). The SiO_2/Al_2O_3 ratio allows for a distinction between high-ratio sandstones and quartz-rich sands, and low-ratio shales (Herron, 1988). With the exception of some of the samples from Gplot, the majority of Sundarbans sediments plot within a mineralogically-stable, silica-depleted litharenite classification. Furthermore, these Sundarbans samples appear to be more mature relative to those of Singh et al. (2005a) and Bhuiyan et al. (2011), indicating that these samples are located further from their source. The presence of the Sundarbans samples in these plots shows that these are also undergoing stronger degrees of weathering, relative to the upper reaches of the GAP and Brahmaputra-Jamuna rivers. A complex relationship exists between tectonic setting and having a unique geochemical signatures, with source and depositional sites having divergent tectonic settings (McLennan et al., 1990; Bahlburg, 1998; Armstrong-Altrin and Verma, 2005).

The enrichment ratios found in the Sundarbans sediments illustrate dissolution during chemical weathering, whereby SiO_2, Na_2O, and K_2O depletion may be attributed to the dissolution of feldspar minerals (Nesbitt and Young, 1984; Singh et al., 2005). Furthermore, increased distance from sediment source, coupled with increased weathering, indicate a depletion of SiO_2 and K_2O in the Sundarbans sediments, relative to what was found by Singh et al. (2005a). The weathering of biotite and ferromagnesium minerals tends to release Mg and K (Clow and Drever, 1996; Singh et al., 2005a; Garzanti et al., 2010; Lupker et al., 2012; Bouchez et al., 2012). The depletion of Na and Ca may be attributed to their highly mobile nature during chemical weathering (Nesbitt and Young, 1984; Singh et al., 2005a; Bouchez et al., 2012). This then results in these elements being concentrated in dissolved river water loads, hence the subsequent depleted nature of these in the Sundarbans samples. The immobility of Ti means that it is enriched in all Sundarbans samples, mainly Lothian and Dhanchi, with a lower enrichment ratio in Gplot, which was found to have a ratio similar to the UCC. Potassium has been found to be less mobile than Ti, and may be associated with clay mineral formation within the GAP whereby K is preferentially adsorbed by clay minerals (cf., Singh et al., 2005a). The enrichment of Fe_2O_3 in the Sundarbans samples may be attributed to weathering and depositional maturity of the Sundarbans, relative to the Gomati River and Brahmaputra-Jamuna sites examined by Singh et al. (2005a) and Bhuiyan et al. (2011), respectively.

The inter-element relationships found in the major element geochemistry show a generally negative trend with SiO_2, indicating a grain-size control on the geochemistry of weathering products (Singh et al., 2005a; Garzanti et al., 2010, 2011; von Eynatten et al., 2012; Lupker et al., 2013). Fe, Al, and Si are considered

immobile elements during Himalayan erosion since they are found to be resistant to chemical weathering (Galy and France-Lanord, 2001; Lupker et al., 2013). The relationship between TiO_2 and Fe_2O_3 was attributed to both enrichment of heavy minerals in Sundarbans sediment and a common source of ferromagnesium minerals. A strong correlation for TiO_2 with Al_2O_3 and K_2O may indicate that Ti was derived from mica in fluvial sediments (Galy and France-Lanord, 2001; Singh et al., 2005a; Lupker et al., 2013). Although the correlation for K_2O was poor (R^2 = 0.06), the correlation with Al_2O_3 was relatively strong (R^2 = 0.66). The poor correlation with K_2O may be attributed to the substitution effect of K with Rb (El-Makky and Sediek, 2012). Singh et al. (2005a) consider correlation between K_2O with MgO and Al_2O_3 (Fig. 10d,f) to reflect illite in suspended sediments. However, this was not found in this study, indicating increased weathering and illite removal within the Sundarbans. The lack of smectite may also be linked to the lack of correlation found between MgO and Al_2O_3, where MgO has weathered out of sediment and dissolved into solution (Fig. 10f). Dissolution of MgO has been found by Singh et al. (2005b) to contribute heavily to the cation budget of the Brahmaputra, where on average 75% of the cations are Ca and Mg.

The A–CN–K ternary diagram and CIA **(**Fig. 11a,b) reveal a trend of increasing weathering throughout the Sundarbans sediments. With progressive chemical weathering, there is an increase in clay mineral composition with a concomitant decrease in feldspars and other minerals (Singh et al., 2005a; Garzanti et al., 2010, 2011; Bouchez et al., 2012; Lupker et al., 2012, 2013). This is further evidenced by Sundarbans sediments following a predicted weathering trend along the A–CN apex of the ternary diagram. The location of both Lothian and Dhanchi samples, along with Gplot samples at the highest point on the A–CN–K ternary

diagram is indicative of higher intensity chemical weathering. The A–CNK–FM ternary diagram (Fig. 11c) illustrates the predominant trend of Sundarbans samples to follow the predicted weathering trend in the GAP as proposed by Singh et al. (2005a). The S/10–CM–NK ternary diagram (Fig. 11d) shows that data plot parallel to the S/10–CM apex, similarly to those Singh et al. (2005a) and Bhuiyan et al. (2011) data. This trend indicates the control of Na and K mobility during weathering (Nesbitt and Young, 1984; Singh et al., 2005a; Garzanti et al., 2011; Lupker et al., 2012; Bouchez et al., 2012). The proximity of the Sundarbans samples to Na and K illustrates the higher degree of weathering in the Sundarbans, compared with Singh et al. (2005a) and Bhuiyan et al. (2011). The primary distinction between Ganges and Brahmaputra sources in the G-B Delta is the degree of weathering in sediments, with Brahmaputra derived sediments being considerably less weathered than those for the Ganges. What this study has shown is that not only are sediments from the Sundarbans more weathered than those found in the Brahmaputra, ruling out a Brahmaputra source of sediment; but that sediments are more intensively weathered than those found by Singh et al. (2005a), with the exception of floodplain and suspended sediments. At the Sundarbans, sediments are considered to be channel sediments, and, given the lithofacies found in this study, may be considered to be intensively weathered.

Chemical mobility within the Sundarbans sediments backs up the inference regarding intense weathering, since increasing weathering intensity is associated with decreasing variability in Si, Na, and K. The rapid decrease in CaO throughout the Sundarbans sediments shows the predominance of Ca to be released during the weathering of feldspars, but not retained in the clay fraction and being dissolved into solution (Singh et al., 2005a). This is supported by Singh et al. (2005b) whereby the

cation budget of the Brahmaputra is dominated by Ca and Mg, with dissolution of CaO increasing as a result of weathering (Fig. 12g). Ca from the Ganges River sediment has been found to be reduced by half from the initial Ca composition (Bouchez et al., 2012).

Zirconium, and its mineral constituent zircon may be related to grain-size variability, whereby Zr has been shown to be correlated with coarse-size fractions (e.g., fine to very-fine sands) (Flood et al., 2016). With increased weathering, there may be a concomitant increase in clay minerals, leading to fining-up in lithofacies.

Sediments in the sites examined in this study are composed of the TMF which are derived from the Ganges River through the GAP, having undergone two cycles of weathering. The provenance and depositional model outlined in this study is both enhanced and adds to the model of Rogers et al. (2013), whereby sedimentation is locally heterogeneous in the Sundarbans with seasonal delivery of sediment distributed throughout all parts. Although Rogers et al. (2013) analysed present-day sedimentation in the Bangladesh Sundarbans, the present study has demonstrated that sediments from the West Bengal Sundarbans are sourced from the GAP, through the Ganges River. As Rogers et al. (2013) have found the majority of sediment deposited on the tidal delta plain during monsoonal activity was derived from flooding. The catchment and upper floodplain may be considered the principal source (i.e., GAP) of sediments accreting on the lower delta plain surface (Rogers et al., 2013).

5.4. Summary of the mineralogy, grain size, and chemical index of alteration from the Sundarbans

The relationship between mineral clusters, GSD facies, and CIA is shown in Fig. 15 from the Lothian, Gplot, and Dhanchi cores. In each core there is a distinct trend, with increasing weathering intensity moving from the base of the core to the core surface shown by the CIA values along with a fining-up in GSD facies. Mineral clusters demonstrate this relationship between mineralogy and GSD facies, with higher quartz, muscovite, and albite indicative of coarse grained sediment, and kaolinite of fine grained sediment (e.g., mineral clusters 6, 4, 2). It has been found that quartz, feldspar, and heavy minerals steadily increase with depth relative to micas, such as muscovite and clay-rich aggregates in the G-B delta (Garzanti et al., 2011). The fluctuations between muscovite mica and quartz reflect most strongly the differentiating settling velocities of sediment, whereby size shifts for micas, which settle slower than quartz in spite of their higher density (Garzanti et al., 2008). In this respect, grain size facies illustrate the continuous fluctuations between slightly coarser, quartz dominated silts, and finer, muscovite mica dominated clays. This is seen with the increase in kaolinite content moving up through each of the cores. Chemical weathering indices have been found to be similar in both the Ganges and Brahmaputra sediments, indicative of significant weathering in monsoonal climates (Garzanti et al., 2011). The CIA for each of the cores shown in Fig. 15 has illustrated the variability in suspension sorting, the weathering indices decrease with depth through the cores from the Sundarbans (cf., Garzanti et al., 2011). This trend in decreasing weathering intensity has been found to be higher in the Ganges plains than in the Brahmaputra (Garzanti et al., 2011). This increase in CIA moving up-core, is understood to be a hydraulic-sorting effect, as a result of decreasing Al, related to phyllosilicates, and increasing Na and Ca, associated with plagioclase, offset by a decrease in K and Mg (Garzanti et al., 2011).

The mineralogy of sediments from the Himalayas is composed primarily of quartz, micas, and feldspars, with the finer fraction composed mainly of phyllosilicates, clay assemblages and hydroxides (Garzanti et al., 2010, 2011; Lupker et al., 2013). During sediment transport these minerals are segregated with coarse-grained quartz enriched in bedload at the bottom of the water column and phyllosilicates and clays found to be enriched in shallow surface waters (Lupker et al., 2013). The sediments of the TMF presented in this study reflect this partitioning of mineralogy and geochemistry as a result of sediment transport.

6. CONCLUSION

The TMF of the Ganges-Brahmaputra Delta have been examined and found to reveal intensively weathered, terrestrial sediment derived from the Ganges River, principally the GAP. The TMF in the West Bengal Sundarbans are composed of sediments sourced from the Ganges that went through initial in-situ weathering, prior to being eroded and chemically weathered in the GAP, and finally being transported to the lower delta plain during the monsoon. The TMF is proposed as being diachronous in terms of the role played by fluvial and marine processes in deposition. The depositional model for the TMF in the far western extent of the G-B delta is that the sediment plume is then transported westwards by prevailing currents, and through tides these sediments are deposited onto the delta plain. This study presents a first-order approximation of lithofacies and geochemistry of the TMF on the western abandoned lower Ganges–Brahmaputra delta and demonstrates that:

1. Geochemical data enhances the weathering model proposed by Singh et al. (2005a), with sediments of the TMF having undergone at least two cycles of weathering.

2. Mineralogy of the cores collected shows a predominance of quartz and mica with clay minerals. Quartz supply is interpreted as indicative of terrestrial sources of sediment, draining the Himalayas.
3. Kaolinite formation is derived from feldspar and muscovite mica with kaolinite the product of intense chemical weathering.
4. Fining upward trend in grain size distributions in the West Bengal Sundarbans.
5. Dhanchi and Lothian Island lithofacies are considered to be muddy tidal flats with Gplot Island indicating an intertidal to shallow subtidal environment with possible channel-mouth and channel-side bar deposits.
6. Geochemical, mineralogical and lithofacies composition of the TMF suggest it is locally heterogeneous with sediment derived from the Ganges and deposited tidally in a low-energy system following the model of Rogers et al. (2013).

ACKNOWLEDGEMENTS

RPF acknowledges the support provided by a Department for Employment and Learning (Northern Ireland) research studentship and the Department of Education and Science's Higher Education Grant Scheme (ROI) via Laois County Council (ROI). RPF also acknowledges the School of Natural and Built Environment (formerly the School of Geography, Archaeology and Palaeoecology), Queen's University, Belfast (QUB) for the fieldwork support provided by their Soulby Research Fund. RPF acknowledges the assistance and technical support provided by Paul O'Meara (PANanalytical B.V.), Mike Dobby (MikeDobby Analytical Consultant), and Pat McBride (QUB), for their help and assistance with XRD, XRF,

and laser granulometry, respectively. RPF and JDO would like to acknowledge the support and assistance of Vincent van Walt and Van Walt Environmental Ltd., in the core extraction and research support, while logistical support in the Sundarbans provided through the Institute of Environmental Studies & Wetland Management (IESWM), Kolkata, West Bengal, India (S. Bhattacharyya and K. Sen Sarma) is gratefully acknowledged. RPF would also like to acknowledge the help and support provided by Mary Bourke of Trinity College Dublin (TCD), Irene Delgado-Fernandez and Breandán Anraoi MacGabhann from Edge Hill University (EHU) for their help and support of this research. The authors would like to acknowledge the helpful comments from the editor of Marine Geology, an anonymous reviewer, and Laura Stutenbecker (Institute of Geological Sciences, University of Bern).

REFERENCES

Adegoke, O.S., Stanley, D.J., 1972. Mica and shell as indicators of energy level and depositional regime on the Nigerian Shelf. Marine Geology, 13, M61–M66.

Aitchison, J., 1986. The Statistical Analysis of Compositional Data: Monographs on Statistics and Applied Probability. Chapman & Hall Ltd., London (436 pp.).

Allen, G.P., Castaing, P., Klingebiel, A., 1972. Distinction of elementary sand populations in the Gironde estuary (France) by R-mode factor analysis of grain-size data. Sedimentology 19, 21–35.

Allen, J.R.L., 1990. Salt-marsh growth and stratification: a numerical model with special reference to the Severn Estuary, southwest Britain. Marine Geology, 95, 77–96.

Allen, J.R.L., 2000. Morphodynamics of Holocene salt marshes: a review sketch from the Atlantic and Southern North Sea coasts of Europe. Quaternary Science Reviews, 19, 1155–1231.

Allison, M.A. 1998a. Geologic framework and environmental status of the Ganges-Brahmaputra delta. Journal of Coastal Research 14, 826–836.

Allison, M.A., 1998b. Historical changes in the Ganges-Brahmaputra delta. Journal of Coastal Research 14, 1269–1275.

Allison, M.A., Kepple, E.B., 2001. Modern sediment supply to the lower delta plain of the Ganges-Brahmaputra River in Bangladesh. Geo-Marine Letters 21, 55–74.

Allison, M.A., Khan, S.R., Goodbred Jr., S.L., Kuehl, S.A., 2003. Stratigraphic evolution of the late Holocene Ganges-Brahmaputra lower delta plain. Sedimentary Geology 155, 317–342.

Andrews, J.T., Vogt, C., 2014. Source to sink: statistical identification of regional variations in the mineralogy of surface sediments in the western Nordic Seas (58°N–75°N; 10°W–40°W). Marine Geology 357, 151–162.

Anthony, E.J., 2015. Wave influence in the construction, shaping and destruction of river deltas: A review. Marine Geology 361, 53–78.

Armstrong-Altrin, J.S., Verma, S.P., 2005. Critical evaluation of six tectonic setting discrimination diagrams using geochemical data of Neogene sediments from known tectonic settings. Sedimentary Geology 177, 115–129.

Auerbach, L.W., Goodbred, Jr., S. L., Mondal, D.R., Wilson, C.A., Ahmed, K.R., Roy, K., Steckler, M.S., Small, C., Gilligan, J.M., Ackerly, B.A., 2015. Flood risk of natural and embanked landscapes on the Ganges–Brahmaputra tidal delta plain. Nature Climate Change 5, 153–157.

Bahlburg H., 1998. The geochemistry and provenance of Ordovician turbidites in the Argentine Puna. In: Panhhurst, R.J., Rapela, C.W, (Eds.). The proto-andean margin of Gondwana. Geological Society of London, Special Paper 142, 127–42.

Barua, D.K., Kuehl, S.A., Miller, R.L., Moore, R.S., 1994. Suspended sediment distribution and residual transport in the coastal ocean off the Ganges – Brahmaputra River mouth. Marine Geology 120, 41–61.

Bass, S.J., Aldridge, J.N., McCave, I.N., Vincent, C.E., 2002. Phase relationships between fine sediment suspensions and tidal currents in coastal seas. Journal of Geophysical Research 107(C10), 3146, doi:10.1029/2001JC001269

Bates, C.C., 1953. Rational theory of delta formation. Bulletin of the American Association of Petroleum Geologists 37, 2119–2162.

Berner, E.K., Berner, R.A., 1996. Global Environment: Water, Air and Geochemical Cycles. Prentice Hall, Inc., Upper Saddle River, NJ.

Bhatia, M.R., 1983. Plate tectonics and geochemical composition of sandstones. The Journal of Geology, 611–627.

Bhattacharyya, S., Pethick, J., Sensarma, K. 2013. Managerial response to sea level rise in the tidal estuaries of the Indian Sundarban: a geomorphological approach. In Xun, W., Whittington, D. (Eds.) Water Policy Journal: Special Edition: The Ganges. Basin Water Policy 15, 51–74.

Bhuiyan, M.A.H., Rahman, M.J.J., Dampare, S.B., Suzuki, S., 2011. Provenance, tectonics and source weathering of modern fluvial sediments of the Brahmaputra–Jamuna River, Bangladesh: inference from geochemistry. Journal of Geochemical Exploration 111, 113–137.

Bickle, M.J., Bunbury, J., Chapman, H.J., Harris, N.B., Fairchild, I.J., Ahmad, T., 2003. Fluxes of Sr into the headwaters of the Ganges. Geochimica et Cosmochimica Acta 67, 2567–2584.

Bish, D.L., 1994. Quantitative X-ray diffraction analysis of soils. In: Amonette, J.E., Zelazny, L.W. (Eds.), Quantitative Methods in Soil Mineralogy. Soil Science Society of America, Madison, USA, pp. 267–295 (Chapter 9).

Bjørlykke, K., 1998. Clay mineral diagenesis in sedimentary basins—a key to the prediction of rock properties. Examples from the North Sea Basin. Clay minerals 33, 15–34.

Boto, K.G., Wellington, J.T., 1984. Soil characteristics and nutrient status in a northern Australian mangrove forest. Estuaries 7, 61–69.

Bouchez, J., Gaillardet, J., Lupker, M., Louvat, P., France-Lanord, C., Maurice, L., Armijos, E., Moquet, J.S., 2012. Floodplains of large rivers: Weathering reactors or simple silos?. Chemical Geology 332, 166–184.

Buggle, B., Glaser, B., Hambach, U., Gerasimenko, N., Marković, S., 2011. An evaluation of geochemical weathering indices in loess–paleosol studies. Quaternary International 240, 12–21.

Canuel, E.A., Martens, C.S., 1993. Seasonal variability in the sources and alteration of organic matter associated with recently deposited sediments. Organic Geochemistry 20, 563–577.

Chakrapani, G.J., 2005. Major and trace element geochemistry in upper Ganga River in the Himalayas, India. Environmental Geology 48, 189–201.

Chakrapani, G.J., Subramanian, V., Gibbs, R.J., Jha, P.K., 1995. Size characteristics and mineralogy of suspended sediments of the Ganges River, India. Environmental Geology 25, 192–196.

Chayes, F., 1960. On correlation between variables of constant sum. Journal of Geophysical Research 6, 4185–4193.

Chayes, F., 1971. Ratio Correlation: A Manual for Students of Petrology and Geochemistry. University of Chicago Press, Chicago (99 pp.).

Chesworth, W., Dejou, J., Larroque, P., 1981. The weathering of basalt and relative mobilities of the major elements at Belbex, France. Geochimica et Cosmochimica Acta 45, 1235–1243.

Clow, D.W., Drever, J.I., 1996. Weathering rates as a function of flow through an alpine soil. Chemical Geology 132, 131–141.

Coleman, J.M., 1969. Brahmaputra River: channel processes and sedimentation. Sedimentary Geology 3, 129–239.

Curray, J.R., 1991. Possible greenschist metamorphism at the base of a 22-km sedimentary section, Bay of Bengal. Geology 19, 1097–1100.

Dalai, T.K., Krishnaswami, S., Sarin, M.M., 2002. Major ion chemistry in the headwaters of the Yamuna river system: Chemical weathering, its temperature dependence and CO_2 consumption in the Himalaya. Geochimica et Cosmochimica Acta 66, 3397–3416.

Dalrymple, R.W., Zaitlin, B.A., Boyd, R.A., 1992. A conceptual model of estuarine sedimentation. Journal of Sedimentary Petrology 62, 1130–1146.

Datta, D.K., Subramanian, V., 1997. Texture and mineralogy of sediments from the Ganges-Brahmaputra-Meghna river system in the Bengal Basin, Bangladesh and their environmental implications. Environmental Geology 30, 181–188.

Dias, J.A., Pilkey, O.H., Heilweil, V.M., 1984. Detrital mica: Environmental significance in North Portugal continental shelf sediments. Comunicações dos Serviços Geológicos de Portugal 70, 93–101.

Doyle, L.J., Cleary, W.J., Pilkey, O.H., 1968. Mica: its use in determining shelf-depositional regimes. Marine Geology 6, 381–389.

Drever, J.I., 1988. The Geochemistry of Natural Waters. Prentice-Hall, Englewood Cliff, NJ.

Dronkers, J., 1986. Tidal asymmetry and estuarine morphology. Netherlands Journal of Sea Research 20, 117–131.

Dutta, M.K., Chowdhury, C., Jana, T.K., Mukhopadhyay, S.K., 2013. Dynamics and exchange fluxes of methane in the estuarine mangrove environment of the Sundarbans, NE coast of India. Atmospheric Environment 77, 631–639.

Ehlmann, A.J., 1968. Clay mineralogy of weathered products and of river sediments, Puerto Rico. Journal of Sedimentary Petrology 38, 885–894.

El-Makky, A.M., Sediek, K.N., 2012. Stream sediments geochemical exploration in the northwestern part of Wadi Allaqi Area, South Eastern Desert, Egypt. Natural resources research 21, 95–115.

Fan, D., Tu, J., Shang, S., Cai, G., 2014. Characteristics of tidal-bore deposits and facies associations in the Qiantang Estuary, China. Marine Geology 348, 1–14.

Flood, R.P., 2014. Post Mid-Holocene Sedimentation of the West Bengal Sundarbans. Unpublished Ph.D. Thesis, Queen's University, Belfast, 646 pp.

Flood, R.P., Bloemsma, M.R., Weltje, G.J., Barr, I.D., O'Rourke, S.M., Turner, J.N. and Orford, J.D., 2016. Compositional data analysis of Holocene sediments from the West Bengal Sundarbans, India: Geochemical proxies for grain-size variability in a delta environment. Applied Geochemistry 75, 222–235.

Flood, R.P., Orford, J.D., McKinley, J.M., Roberson, S., 2015. Effective grain size distribution analysis for interpretation of tidal–deltaic facies: West Bengal Sundarbans. Sedimentary Geology 318, 58–74.

Fontorbe, G., Christina, L., Chapman, H.J. Bickle, M.J., 2013. The silicon isotopic composition of the Ganges and its tributaries. Earth and Planetary Science Letters 381, 21–30.

Frings, P.J., Clymans, W., Fontorbe, G., Gray, W., Chakrapani, G., Conley, D.J., De La Rocha, C., 2015. Silicate weathering in the Ganges alluvial plain. Earth and Planetary Science Letters 427, 136–148.

Fritz, S.J., Mohr, D.W., 1984. Chemical alteration in the micro weathering environment within a spheroidally-weathered anorthosite boulder. Geochimica et Cosmochimica Acta 48, 2527–2535.

Galán, E., Gómez-Ariza, J.L., González, I., Fernández-Caliani, J.C., Morales, E., Giráldez, I., 2003. Heavy metal partitioning in river sediments severely

polluted by acid mine drainage in the Iberian Pyrite Belt. Applied Geochemistry 18, 409–421.

Galy, A., France-Lanord, C., 1999. Weathering processes in the Ganges–Brahmaputra basin and the riverine alkalinity budget. Chemical Geology 159, 31–60.

Galy, A., France-Lanord, C., 2001. Higher erosion rates in the Himalaya: Geochemical constraints on riverine fluxes. Geology 29, 23–26.

Garzanti, E., Andò, S. and Vezzoli, G., 2008. Settling equivalence of detrital minerals and grain-size dependence of sediment composition. Earth and Planetary Science Letters 273, 138–151.

Garzanti, E., Andó, S., France-Lanord, C., Censi, P., Vignola, P., Galy, V., Lupker, M., 2011. Mineralogical and chemical variability of fluvial sediments 2. Suspended-load silt (Ganga–Brahmaputra, Bangladesh). Earth and Planetary Science Letters 302, 107–120.

Garzanti, E., Andò, S., France-Lanord, C., Vezzoli, G., Censi, P., Galy, V., Najman, Y., 2010. Mineralogical and chemical variability of fluvial sediments: 1. Bedload sand (Ganga–Brahmaputra, Bangladesh). Earth and Planetary Science Letters 299, 368–381.

Garzanti, E., Andò, S., Vezzoli, G., 2009. Grain-size dependence of sediment composition and environmental bias in provenance studies. Earth and Planetary Science Letters 277, 422–432.

Giri, C., Pengra, B., Zhu, Z., Singh, A., Tieszen, L.L., 2007. Monitoring mangrove forest dynamics of the Sundarbans in Bangladesh and India using multi-temporal satellite data from 1973 to 2000. Estuarine, Coastal and Shelf Science 73, 91–100.

Goodbred Jr., S.L. 2003. Response of the Ganges dispersal system to climate change: a source-to-sink view since the last interstade. Sedimentary Geology 162, 83–104.

Goodbred Jr., S.L., Kuehl, S.A., 2000a. The significance of large sediment supply, active tectonism and eustasy on margin sequence development: Late Quaternary stratigraphy and evolution of the Ganges-Brahmaputra delta. Sedimentary Geology 133, 227–248.

Goodbred Jr., S.L., Kuehl, S.A., 2000b. Enormous Ganges-Brahmaputra sediment discharge during strengthened early Holocene monsoon. Geology 28, 1083–1086.

Goodbred Jr., S.L., Kuehl, S.A., Steckler, M.S., Sarker, M.H. 2003. Controls on facies distribution and stratigraphic preservation in the Ganges–Brahmaputra delta sequence. Sedimentary Geology 155, 301–316.

Goodbred, S.L., Paolo, P.M., Ullah, M.S., Pate, R.D., Khan, S.R., Kuehl, S.A., Singh, S.K., Rahaman, W., 2014. Piecing together the Ganges-Brahmaputra-Meghna River delta: Use of sediment provenance to reconstruct the history and interaction of multiple fluvial systems during Holocene delta evolution. Geological Society of America Bulletin 126, 1495–1510.

Goodbred, S.L., Saito, Y., 2011. Tide-dominated Deltas. In: Davis, R. Dalyrymple, R.W. (Eds.) Principles of Tidal Sedimentology. Springer, New York, pp. 129–149.

Grant, W.H., 1963. Weathering of Stone Mountain Granite. In Ingersoll, E.C. ed. Clays and Clay Minerals, v. 11, pp. 65-73.

Gutierrez, M., 2005. Climatic Geomorphology. Elsevier, Amsterdam.

Hait, A.K., Das, J.K., Ghosh, S., Ray, A.K., Saha, A.K., Chanda, S., 1996. New dates of Pleisto-Holocene subcrop samples from south Bengal, India. Indian Journal of Earth Sciences 23, 79–82.

Hart, M.G.R., 1959. Sulphur oxidation in tidal mangrove soils of Sierra Leone. Plant and Soil 11, 215–236.

Helsel, D.R., 2005. Nondetects and Data Analysis: Statistics for Censored Environmental Data. John Wiley and Sons, New York (250 pp.).

Heroy, D.C., Kuehl, S.A. Goodbred, S.L., 2003. Mineralogy of the Ganges and Brahmaputra Rivers: implications for river switching and Late Quaternary climate change. Sedimentary Geology 155, 343–359.

Herron, M.M., 1988. Geochemical classification of terrigeneous sands and shales from core or log data. Journal of Sedimentary Petrology 58, 820–829.

Hesse, P.R., 1961. Some differences between the soils of Rhizophora and Avicennia mangrove swamps in Sierra Leone. Plant and Soil 14, 335–346.

Hillier, S., 2000. Accurate quantitative analysis of clay and other minerals in sandstones by XRD: comparison of a Rietveld and a reference intensity ratio (RIR) method and the importance of sample preparation. Clay Minerals 35, 291–302.

Hinman, N.W., 1998. Sequences of silica phase transitions: effects of Na, Mg, K, Al, and Fe ions. Marine Geology 147, 13–24.

Hübscher, C., Breitzke, M., Michels, K., Kudrass, H.R., Spiess, V., Wiedicke, M., 1998. Late Quaternary seismic stratigraphy of the eastern Bengal Shelf. Marine Geophysical Researches 20, 57–71.

Hughes, Z.J., 2011. Tidal Channels on Tidal Flats and Marshes. In Davis, R.A., Dalrymple, R.W. (Eds.) Principles of tidal sedimentology. Springer, New York, pp. 269–300.

ICDD, 2002. International Centre for Diffraction Data. Mineral Powder diffraction file data book. (941 p.).

Islam, M.R., Stuart, R., Risto, A., Vesa, P., 2002. Mineralogical changes during intense chemical weathering of sedimentary rocks in Bangladesh. Journal of Asian Earth Sciences 20, 889–901.

Johnson, M.R.W., 1994. Volume balance of erosional loss and sediment deposition related to Himalayan uplifts. Journal of the Geological Society 151, 217–220.

Johnson, S.Y., Alam, A.M.N., 1991. Sedimentation and tectonics of the Sylhet trough, Bangladesh. Geological Society of America Bulletin 103, 1513–1527.

Kabata-Pendias, A., Pendias, H., 2000. Trace elements in soils and plants. 3rd ed. Boca Raton, Florida; London: CRC Press, 413 p.

Kuehl, S.A., Hariu, T.M. and Moore, W.S., 1989. Shelf sedimentation off the Ganges-Brahmaputra river system: Evidence for sediment bypassing to the Bengal fan. Geology 17, 1132–1135.

Kuehl, S.A., Levy, B.M., Moore, W.S. and Allison, M.A., 1997. Subaqueous delta of the Ganges-Brahmaputra river system. Marine Geology 144, 81–96.

Lindsay, J.F., Holliday, D.W., Hulbert, A.G., 1991. Sequence Stratigraphy and the Evolution of the Ganges-Brahmaputra Delta Complex (1). AAPG Bulletin 75, 1233–1254.

Lupker, M., France-Lanord, C., Galy, V., Lavé, J., Gaillardet, J., Gajurel, A.P., Guilmette, C., Rahman, M., Singh, S.K. and Sinha, R., 2012. Predominant

floodplain over mountain weathering of Himalayan sediments (Ganga basin). Geochimica et Cosmochimica Acta 84, 410–432.

Lupker, M., France-Lanord, C., Galy, V., Lavé, J., Kudrass, H., 2013. Increasing chemical weathering in the Himalayan system since the Last Glacial Maximum. Earth and Planetary Science Letters 365, 243–252.

McLaren, P., Bowles, D., 1985. The effects of sediment transport on grain-size distributions. Journal of Sedimentary Research 55, 0457–0470.

McLennan, S.M., 1995. Sediments and soils: chemistry and abundances. In: Ahrens, T.J. (Ed.), Rock Physics and Phase Relations: A Handbook of Physical Constants, vol. 3. American Geophysical Union Reference Shelf, 8–19.

McLennan, S.M., Taylor, S.R., McCulloch, M.T., Maynard, J.B., 1990. Geochemical and Nd–Sr isotopic composition of deep-sea turbidites: crustal evolution and plate tectonic associations. Geochimica et Cosmochimica Acta 54, 2015–2050.

Middelburg, J.J., Nieuwenhuize, J., Slim, F.J., Ohowa, B., 1996. Sediment biogeochemistry in an East African mangrove forest (Gazi bay, Kenya). Biogeochemistry 34, 133–155.

Morgan, J.P. and McIntire, W.G., 1959. Quaternary geology of the Bengal basin, East Pakistan and India. Geological Society of America Bulletin 70, 319–342.

Mukherjee, A., Fryar, A.E., Thomas, W.A., 2009. Geologic, geomorphic and hydrologic framework and evolution of the Bengal basin, India and Bangladesh. Journal of Asian Earth Sciences 34, 227–244.

Nesbitt, H.W., 1979. Mobility and fractionation of rare earth elements during weathering of a granodiorite. Science 279, 206–210.

Nesbitt, H.W., Markovics, G., 1980. Chemical processes affecting alkalis and alkaline earths during continental weathering. Geochimica et Cosmochimica Acta 44, 1659–1666.

Nesbitt, H.W., Young, G.M., 1982. Early Proterozoic climates and plate motions inferred from major element chemistry of lutites. Nature 299, 715–717.

Nesbitt, H.W., Young, G.M., 1989. Formation and diagenesis of weathering profiles. The Journal of Geology 129–147.

Nesbitt, H.W., Young, G.M., McLennan, S.M., Keays, R.R., 1996. Effects of chemical weathering and sorting on the petrogenesis of siliciclastic sediments, with implications for provenance studies. The Journal of Geology 104, 525–542.

Pearson, K., 1896. On the form of spurious correlations which may arise when indices are used in the measurement of organs. Proceedings of the Royal Society of London 60, 489–502.

Pecharsky, V.K., Zavalij, P.Y., 2009. Fundamentals of powder diffraction and structural characterization of materials, 2nd edn., New York: Springer, 768 p.

Pethick, J.S., 1980. Velocities, surges and asymmetry in tidal channels. Estuarine, Coastal and Marine Science 11, 331–345.

Pethick, J.S., Orford, J.D., 2013. Rapid rise in effective sea-level in southwest Bangladesh: Its causes and contemporary rates. Global and Planetary Change 111, 237–245.

Pettijohn, F., Potter, P., Siever, R., 1972. Sand and Sandstone: New York, Springer-Verlag, 618 p.

Pomerancblum, M., 1966. The distribution of heavy minerals and their hydraulic equivalents in sediments of the Mediterranean continental shelf of Israel. Journal of Sedimentary Petrology 36, 162–174.

Potter, P.E., 1978. Petrology and chemistry of modern big river sands. The Journal of Geology 86, 423–449.

Prins, M.A., Postma, G. 2000. Effects of climate, sea level, and tectonics unraveled for last deglaciation turbidite records of the Arabian Sea. Geology 28, 375–378.

Purkait, B., Majumdar, D.D., 2014. Distinguishing different sedimentary facies in a deltaic system. Sedimentary Geology 308, 53–62.

R Development Core Team, 2011. R: A Language and Environment for Statistical Computing. Compositional Data Analysis in the Geosciences — From Theory to Practice. R Foundation for Statistical Computing, Vienna Available online at http://www.Rproject.org/. (last accessed 13.12.2014.).

Rengarajan, R., Singh, S.K., Sarin, M.M. and Krishnaswami, S., 2009. Strontium isotopes and major ion chemistry in the Chambal River system, India: implications to silicate erosion rates of the Ganga. Chemical Geology 260, 87–101.

Rengarajan, R., Singh, S.K., Sarin, M.M. Krishnaswami, S., 2009. Strontium isotopes and major ion chemistry in the Chambal River system, India: implications to silicate erosion rates of the Ganga. Chemical Geology 260, 87–101.

Rietveld, H., 1969. A profile refinement method for nuclear and magnetic structures. Journal of applied Crystallography 2, 65–71.

Rietveld, H.M., 1967. Line profiles of neutron powder-diffraction peaks for structure refinement. Acta Crystallographica 22, 151–152.

Roberson, S., Weltje, G.J., 2014. Inter-instrument comparison of particle-size analysers. Sedimentology 61, 1157–1174.

Rogers, K.G., Goodbred Jr., S.L., Mondal, D.R., 2013. Monsoon sedimentation on the 'abandoned' tide-influenced Ganges-Brahmaputra delta plain. Estuarine, Coastal and Shelf Science 131, 297–309.

Roser, B.P., Korsch, R.J., 1986. Determination of tectonic setting of sandstone-mudstone suites using content and ratio. The Journal of Geology 94, 635–650.

Salminen, R., Batista, M.J., Bidovec, M., Demetriades, A., De Vivo, B., De Vos, W., Duris, M., Gilucis, A., Gregorauskiene, V., Halamic, J., Heitzmann, P., Lima, A., Jordan, G., Klaver, G., Klein, P., Lis, J., Locutura, J., Marsina, K., Mazreku, A., O'Connor, P.J., Olsson, S.Å., Ottesen, R.-T., Petersell, V., Plant, J.A., Reeder, S., Salpeteur, I., Sandström, H., Siewers, U., Steenfelt, A., Tarvainen, T., 2005. Geochemical Atlas of Europe. Part 1: Background Information, Methodology and Maps. Geological Survey of Finland, Espoo downloaded at 01.11.2016 http://www.gtk.fi/publ/foregsatlas.

Sarin, M.M., Krishnaswami, S., Dilli, K., Somayajulu, B.L.K. and Moore, W.S., 1989. Major ion chemistry of the Ganga-Brahmaputra river system: Weathering processes and fluxes to the Bay of Bengal. Geochimica et Cosmochimica Acta 53, 997–1009.

Sarkar, A., Sengupta, S.M.J.M., McArthur, J.M., Ravenscroft, P., Bera, M.K., Bhushan, R., Samanta, A. and Agrawal, S., 2009. Evolution of Ganges–Brahmaputra western delta plain: clues from sedimentology and carbon isotopes. Quaternary Science Reviews 28, 2564–2581.

Sarkar, S.K., Frančišković-Bilinksi, S., Bhattacharya, A., Saha, M., Bilinski, H., 2004. Levels of elements in the surficial estuarine sediments of the Hugli River, northeast India and their environmental implications. Environment International 30, 1089–1098.

Schimanski, A., Stattegger, K., 2005. Deglacial and Holocene evolution of the Vietnam shelf: stratigraphy, sediments and sea-level change. Marine Geology 214, 365–387.

Sheldon, N.D., Tabor, N.J., 2009. Quantitative paleoenvironmental and paleoclimatic reconstruction using paleosols. Earth-Science Reviews 95, 1–52.

Singh, M., Sharma, M. and Tobschall, H.J., 2005a. Weathering of the Ganga alluvial plain, northern India: implications from fluvial geochemistry of the Gomati River. Applied Geochemistry 20, 1–21.

Singh, S.K., Sarin, M.M. and France-Lanord, C., 2005b. Chemical erosion in the eastern Himalaya: major ion composition of the Brahmaputra and $\delta^{13}C$ of dissolved inorganic carbon. Geochimica et Cosmochimica Acta 69, 3573–3588.

Small, C., Steckler, M., Seeber, L., Akhter, S.H., Goodbred, S., Mia, B. and Imam, B., 2009. Spectroscopy of sediments in the Ganges–Brahmaputra delta: Spectral effects of moisture, grain size and lithology. Remote Sensing of Environment 113, 342–361.

Snyder, R.L., Bish, D.L., 1989. Quantitative analysis. In: Bish, D.L., Post, J.E. (Eds), Modern Powder Diffraction, Reviews in Mineralogy, Volume 20, Mineralogical Society of America, USA, 101–144 (Chapter 5).

Stallard, R.F., 1988. Weathering and erosion in the Humid tropics. In: Lerman, A., Meybeck, M. (Eds.), Physical and Chemical Weathering in Geochemical Cycles. Kluwer, Dodretch, 225–246.

Stanley, D.J., Hait, A.K., 2000. Deltas, radiocarbon dating, and measurements of sediment storage and subsidence. Geology 28, 295–298.

Stoch, L., Sikora, W., 1976. Transformations of micas in the process of kaolinitization of granites and gneisses. Clays and Clay Minerals 24, 156–162.

Taylor, S.R. and McLennan, S.M., 1985. The continental crust: its composition and evolution. Oxford, Blackwell, London, 312 + XV p.

Thomas, M.F., 2003. Late Quaternary sediment fluxes from tropical watersheds. Sedimentary Geology 162, 63–81.

Twilley, R.R., 1988. Coupling of mangroves to the productivity of estuarine and coastal waters. In: Jansson, B.O. (Ed.) Coastal offshore Ecosystem: Interactions. Lecture Notes on Coastal and Estuarine Studies, vol. 22. Springer-Verlag, Berlin, pp. 155–180.

Umitsu, M., 1987. Late Quaternary sedimentary environment and landform evolution in the Bengal lowland: Geographical Review of Japan 60, 164–178.

Umitsu, M., 1993. Late Quaternary sedimentary environments and landforms in the Ganges delta: Sedimentary Geology 83, 177–186.

von Eynatten, H., Tolosana-Delgado, R., Karius, V., 2012. Sediment generation in modern glacial settings: grain-size and source-rock control on sediment composition. Sedimentary Geology 280, 80–92.

Ward, J.H., 1963. Hierarchical grouping to optimize an objective function. Journal of the American Statistical Association 58, 236–244.

Wedepohl K.H., 1978. Handbook of Geochemistry 11, Sections 73, B-G. Springer-Verlag.

Wells, J.T., 1995. Tide-Dominated Estuaries and Tidal Rivers. In: Perillo, G.M. (Ed.) Geomorphology and sedimentology of estuaries – Developments in Sedimentology, vol. 53. Elsevier, Amsterdam, 179–206.

Weltje, G.J., Prins, M.A., 2003. Muddled or mixed? Inferring palaeoclimate from size distributions of deep-sea clastics. Sedimentary Geology 162, 39–62.

Weltje, G.J., Prins, M.A., 2007. Genetically meaningful decomposition of grain-size distributions. Sedimentary Geology 202, 409–424.

List of tables

List of figures

phyllosilicates, respectively. Linear trend in mineralogical sorting is indicative of transportation. Gray ellipses indicate composition of source area: the Himalaya and the Siwaliks (Galy and France-Lanord, 2001). Star corresponds to average UCC (Taylor and McLennan, 1985). CS: channel sediments, FS: flood sediments, and SS: suspended sediments. *Data points from Singh et al. (2005a), **average data points from Singh et al. (2005a), ***average data points from Bhuiyan et al. (2011)

Fig. 7 Geochemical classification diagrams of the West Bengal Sundarbans sediments along with data from Singh et al. (2005a) and Bhuiyan et al. (2011) from (a) Pettijohn et al. (1972) and (b) Herron (1988). CS: channel sediments, FS: flood sediments, and SS: suspended sediments. *Data points from Singh et al. (2005a), **average data points from Singh et al. (2005a), ***average data points from Bhuiyan et al. (2011)

Fig. 8 Tectonic discrimination diagram for the West Bengal Sundarbans sediments. Boundaries of fields are from Roser and Korsch (1986). CS: channel sediments, FS: flood sediments, and SS: suspended sediments. *Data points from Singh et al. (2005a), **average data points from Singh et al. (2005a), ***average data points from Bhuiyan et al. (2011)

Fig. 9 Element ratio of West Bengal Sundarbans sediments calculated from average major element concentrations normalised to UCC (Taylor and McLennan, 1985) with respect to Al_2O_3 (Eq. 2). CS: channel sediments, FS: flood sediments, and SS: suspended sediments. **Average data points from Singh et al. (2005a), ***average data points from Bhuiyan et al. (2011)

Fig. 10 Variation diagrams of major elements in West Bengal Sundarbans sediments, data are plotted against Al_2O_3, SiO_2 and TiO_2. For reference, UCC and World

Sediments were also plotted as grey circle and cross, respectively, with **average data points from Singh et al. (2005a), ***average data points from Bhuiyan et al. (2011). CS: channel sediments, FS: flood sediments, and SS: suspended sediments

Fig. 11 (a) A–CN–K ternary diagram of molecular proportions showing sediment suites from the West Bengal Sundarbans. A = Al_2O_3; C = CaO; N = Na_2O and K = K_2O. Also plotted is the UCC (Taylor and McLennan, 1985) in a grey cross, along with idealised mineral compositions. Shown are the predicted weathering trends exhibited by the Ganga alluvial plain with arrows, which had experienced incipient to moderate chemical weathering. (b) Bar plot of average Chemical Index of Alteration (Eq. 1) values of the West Bengal Sundarbans sediments along with Singh et al. (2005a) and Bhuiyan et al. (2011) for comparative purposes. (c) A–CNK–FM and (d) S/10–CM–NK ternary diagrams showing sediment suites from the West Bengal Sundarbans. A = Al_2O_3; C = CaO; N = Na_2O; K = K_2O; F = Total Fe; M = MgO; S = SiO_2.

Fig. 12 Chemical mobility in the West Bengal Sundarbans sediments during weathering processes, calculated in terms of percentage change (normalised with respect to TiO_2) of individual major/trace elements vs. progressive degree of chemical alteration (CIA values) (Eq. 3)

Fig. 13 Cartoon example of depositional model for the far western extent of the Ganges-Brahmaputra delta in the West Bengal Sundarbans. The TMF is proposed as being a diachronous facies unit whereby fluvial dominance was prevalent c. 5,000 yrs BP that gradually developed into a mixed fluvio-tidal dominant delta from c. 3,000 yrs BP, to finally its current state as being a tidal dominant delta. Sediment is sourced primarily from the Ganges river and

delivered to the coastal shelf as a dominantly monsoonal plume that is re-worked onto the delta plain, with the emerging tidal supplied sediment plume thinning in volume and sediment size as it is carried further west to the tidal dominant delta (figure not to scale)

Fig. 14 (a) kaolinite and muscovite regression of XRD cluster representative samples. A strong positive correlation ($R^2 = 0.90$) is found between these clay and mica mineral compositions, indicative of weathering of mica. (b) kaolinite and quartz regression of cluster representative samples. A strong negative correlation ($R^2 = –0.96$) is found between kaolinite and quartz, indicative of grain-size variability

Fig. 15 Mineralogy, grain size distribution (GSD) facies, and chemical index of alteration (CIA) from the Lothian, Gplot, and Dhanchi Island cores, with Lothian Island GSD adapted from Flood et al. (2015)

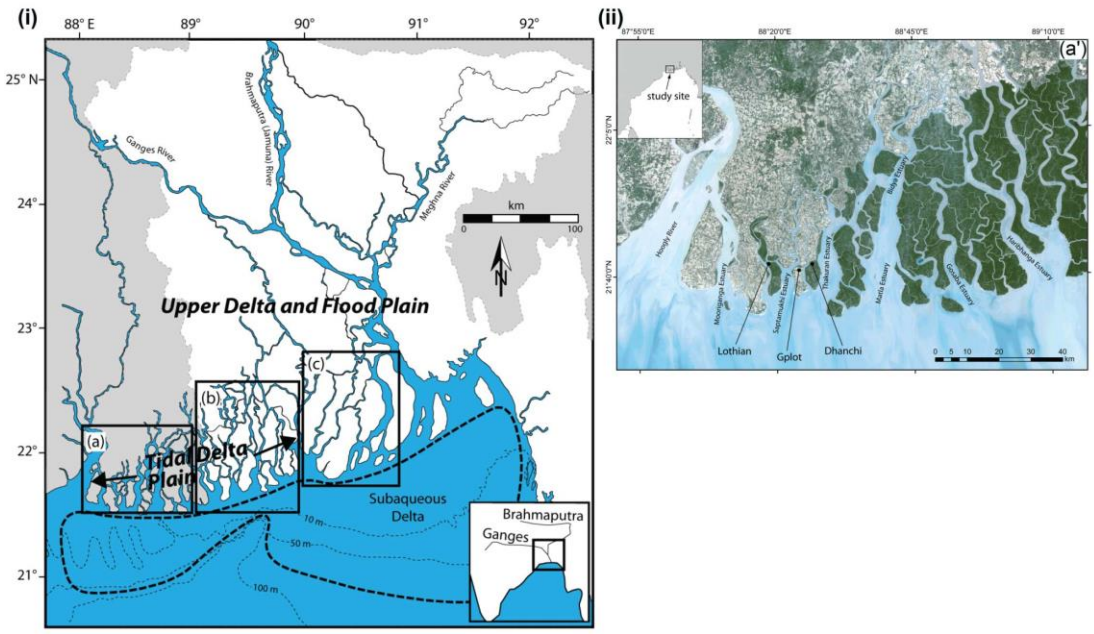

Fig. 1

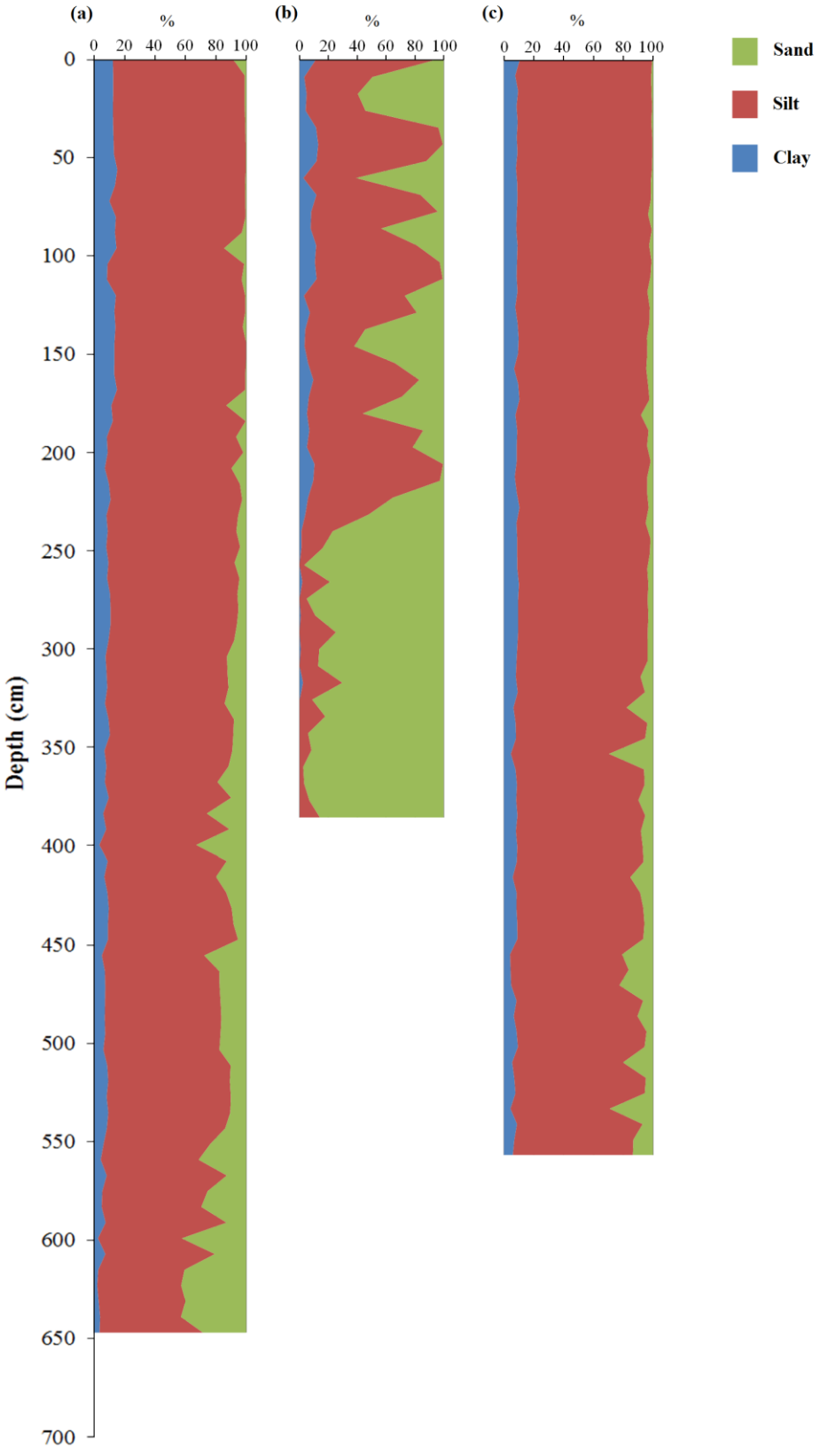

Fig. 2

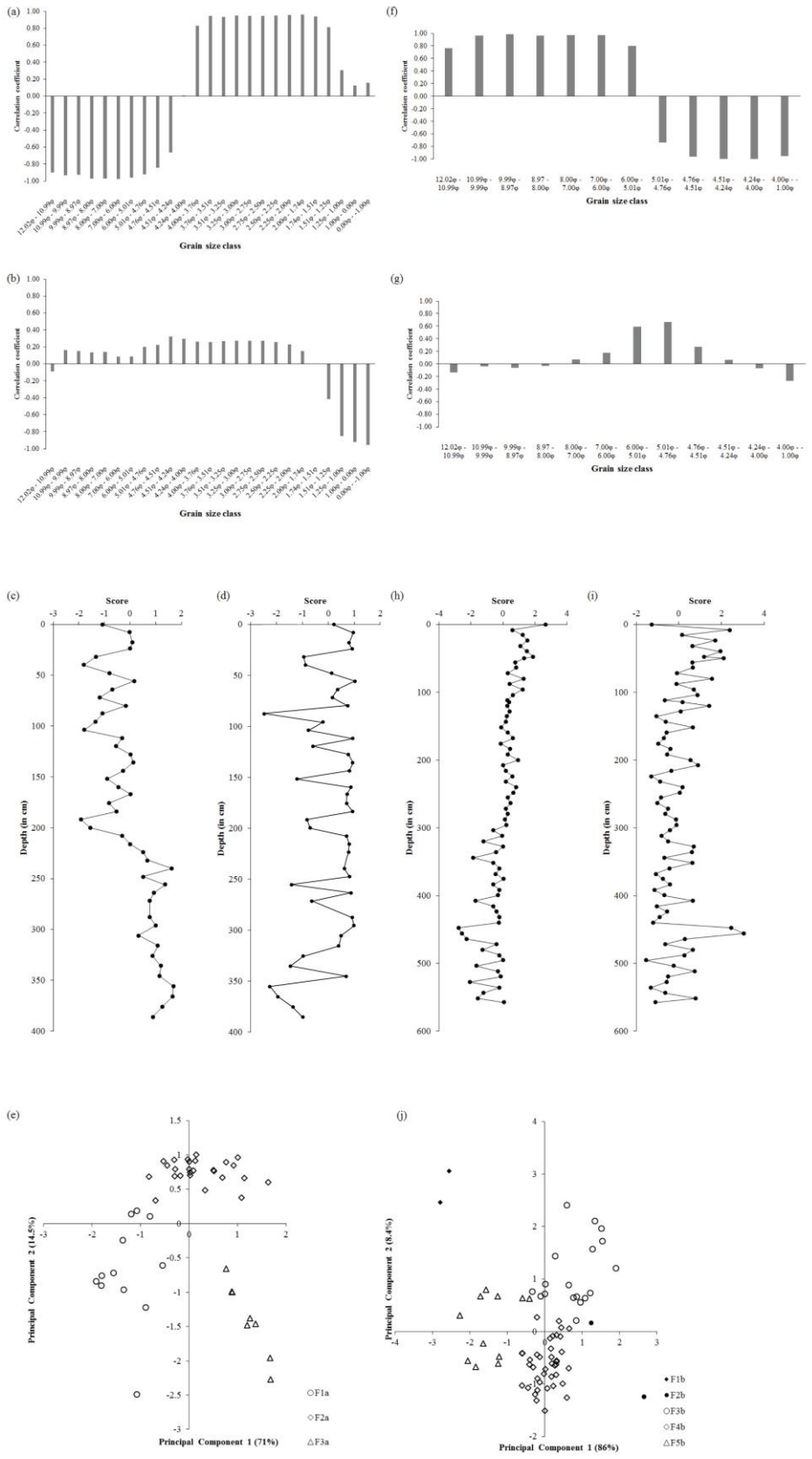

Fig. 3

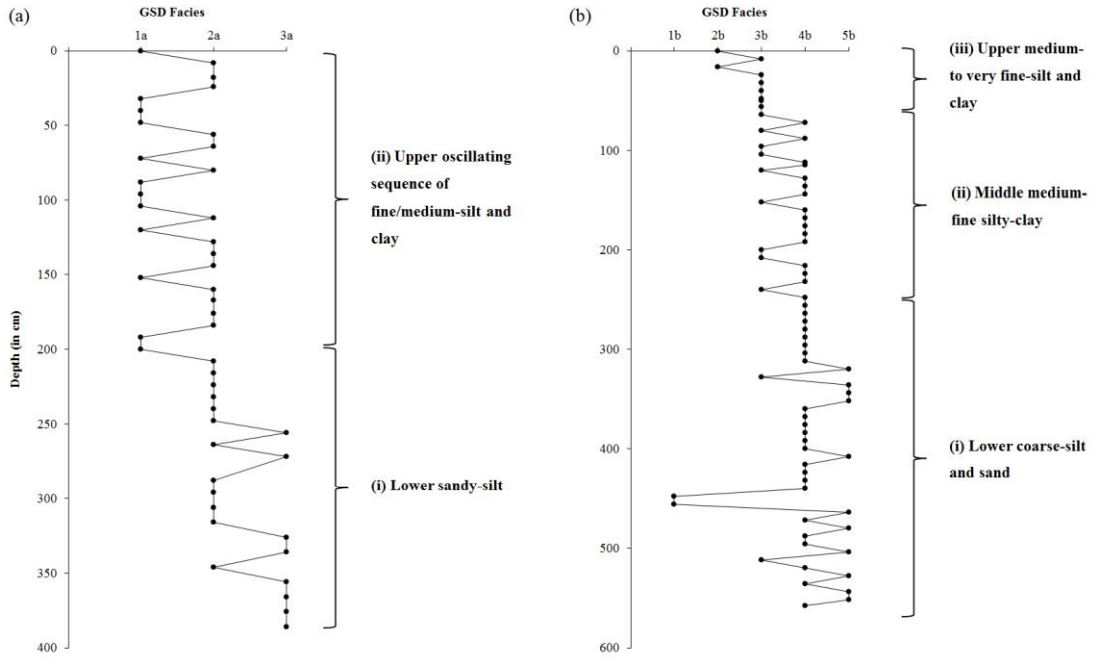

Fig. 4

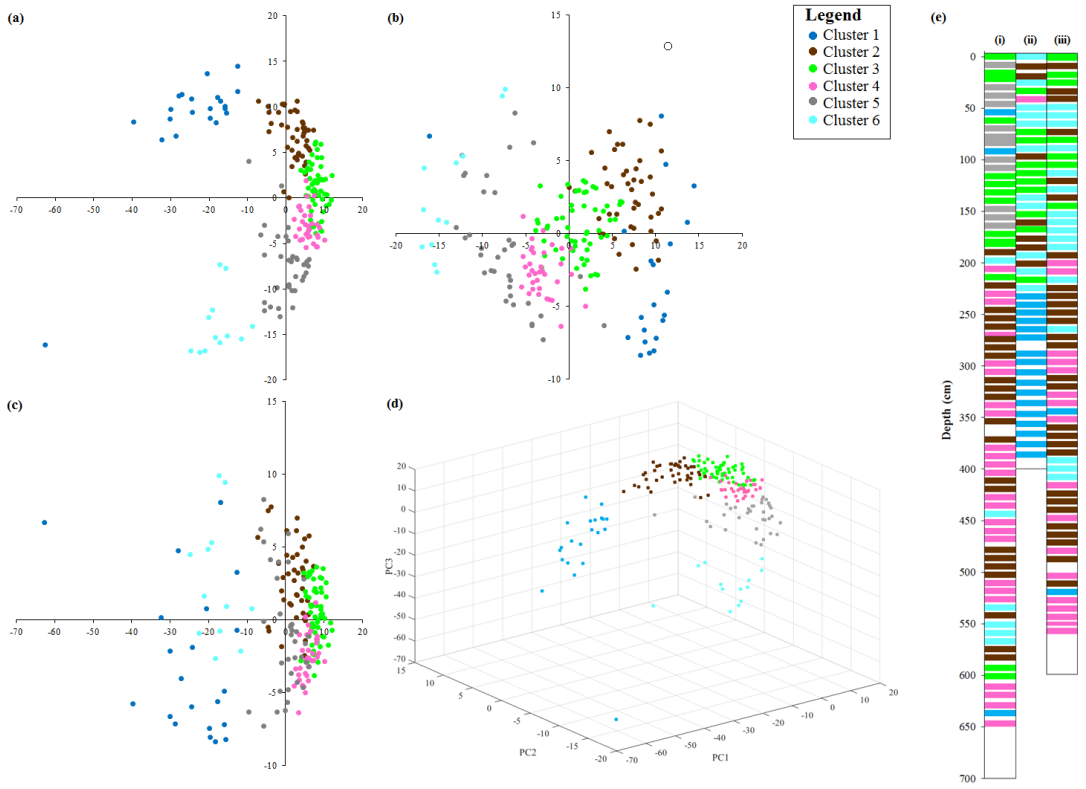

Fig. 5

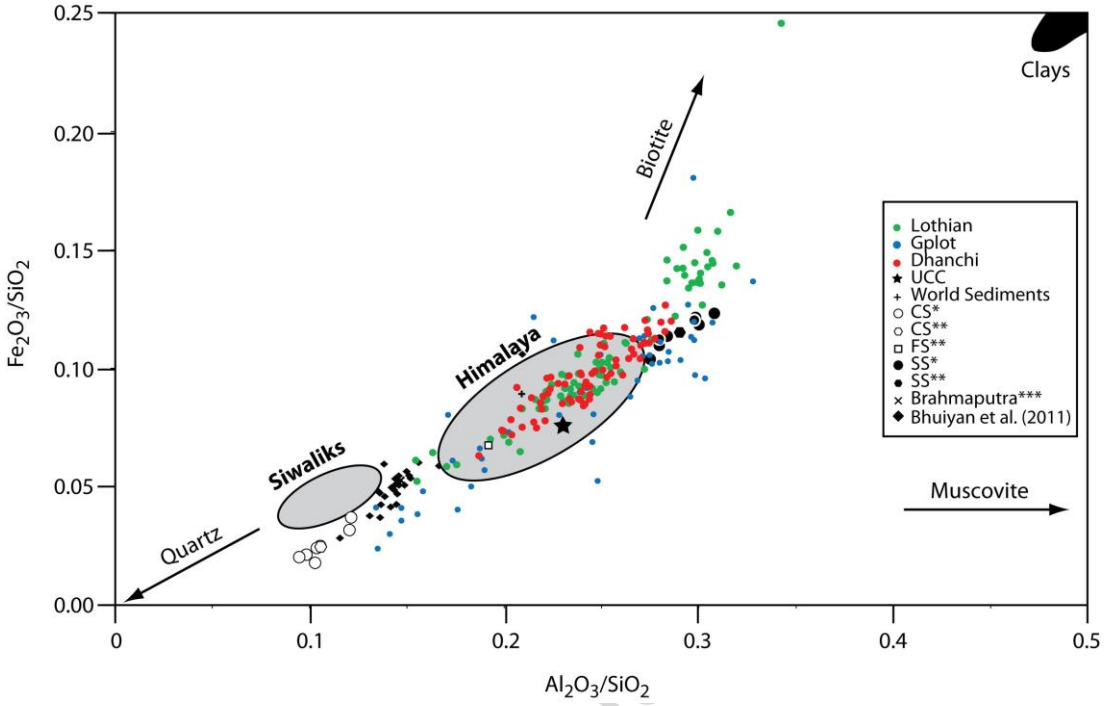

Fig. 6

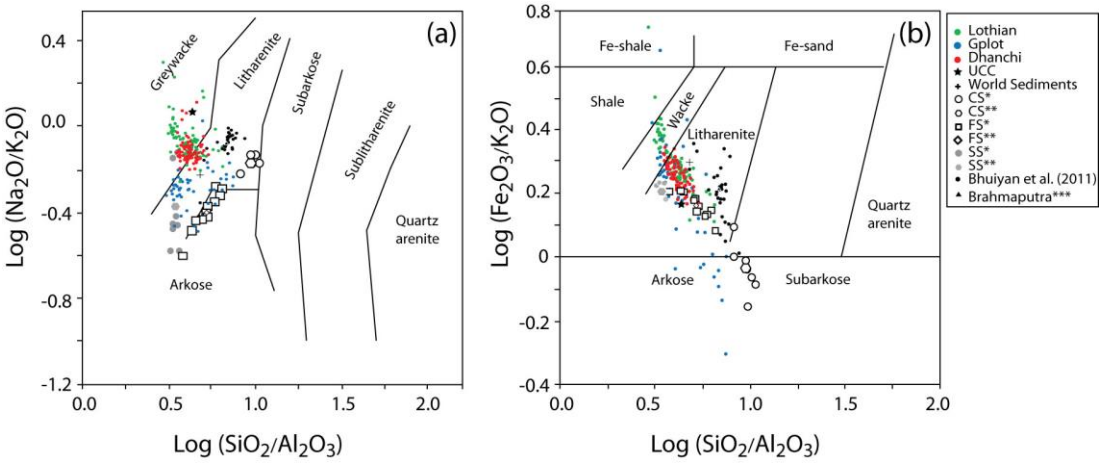

Fig. 7

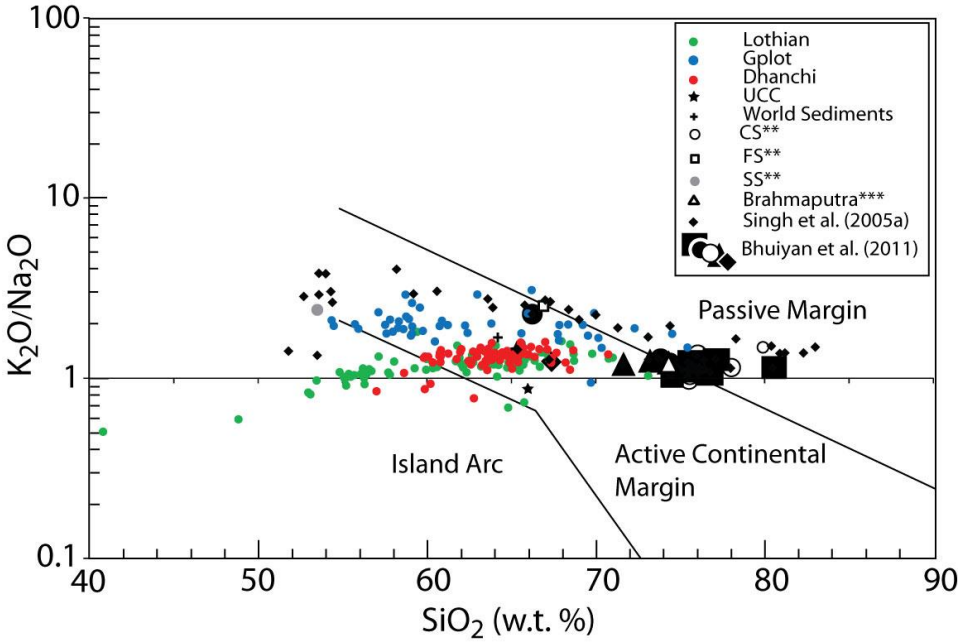

Fig. 8

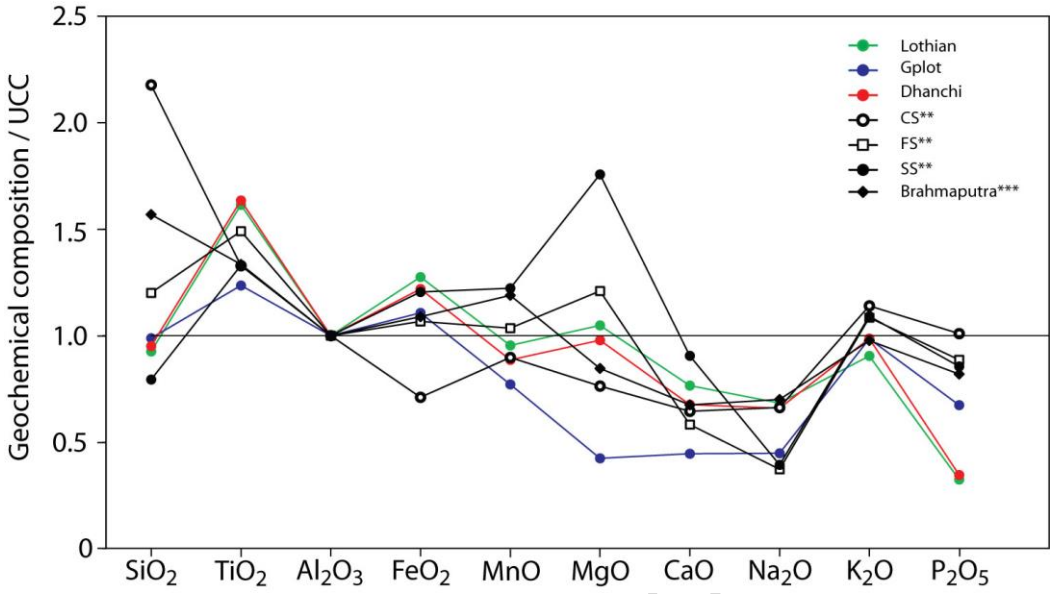

Fig. 9

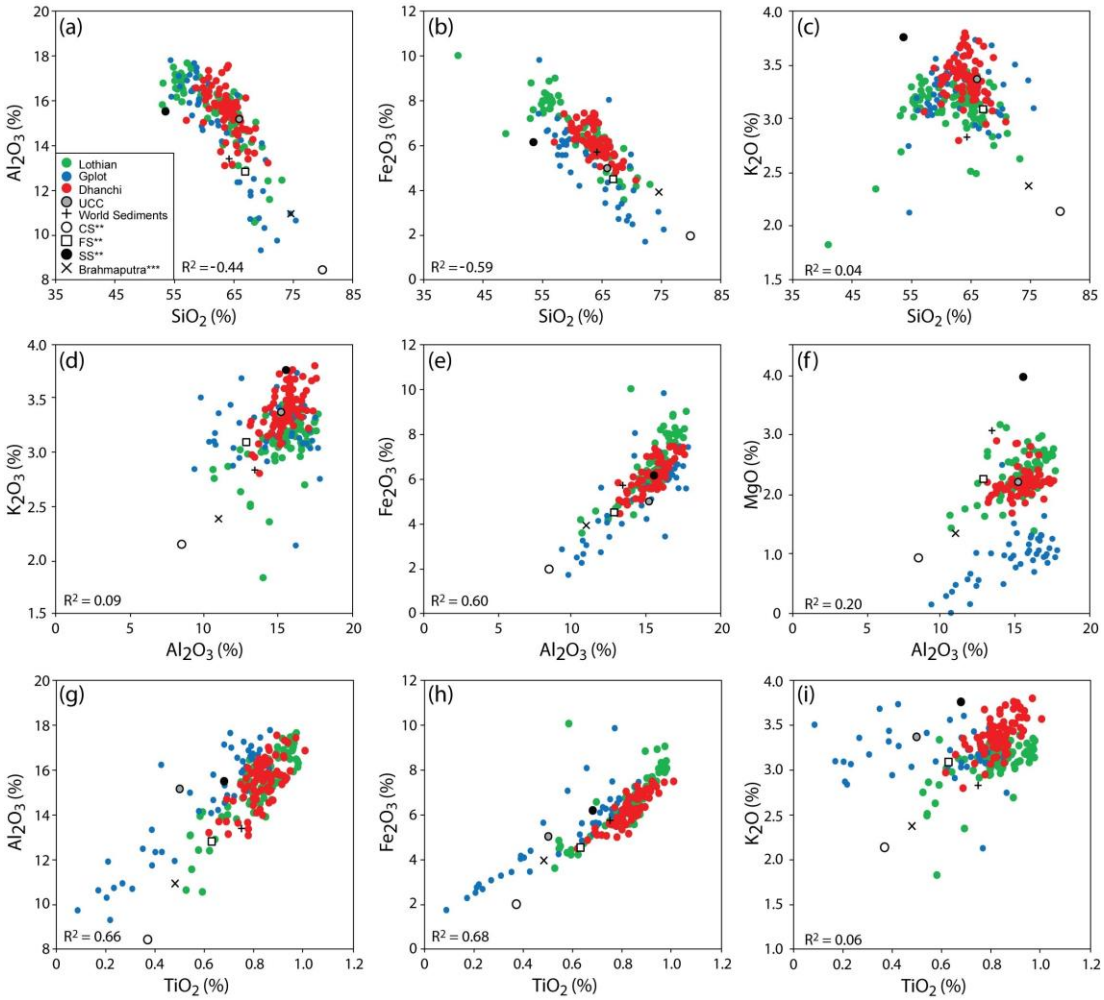

Fig. 10

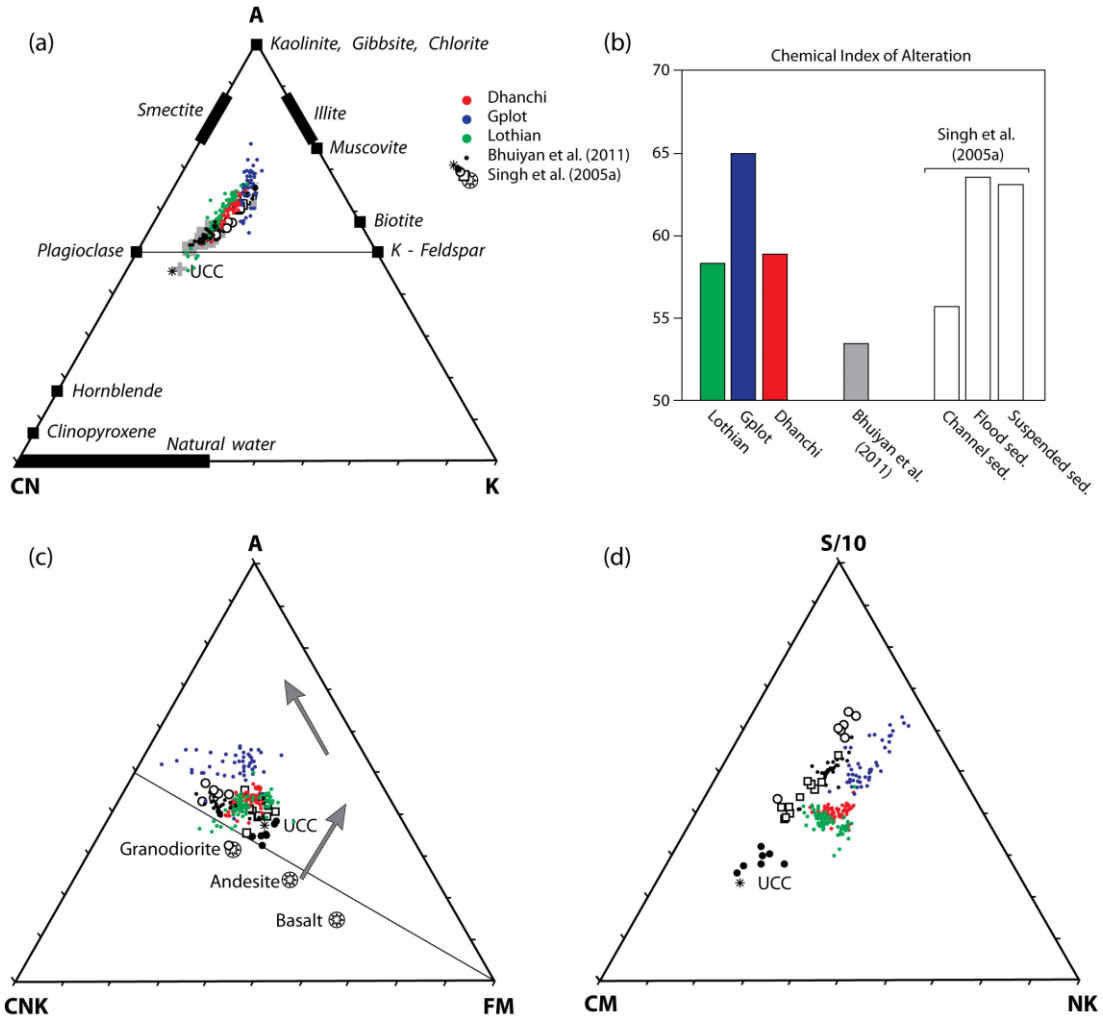

Fig. 11

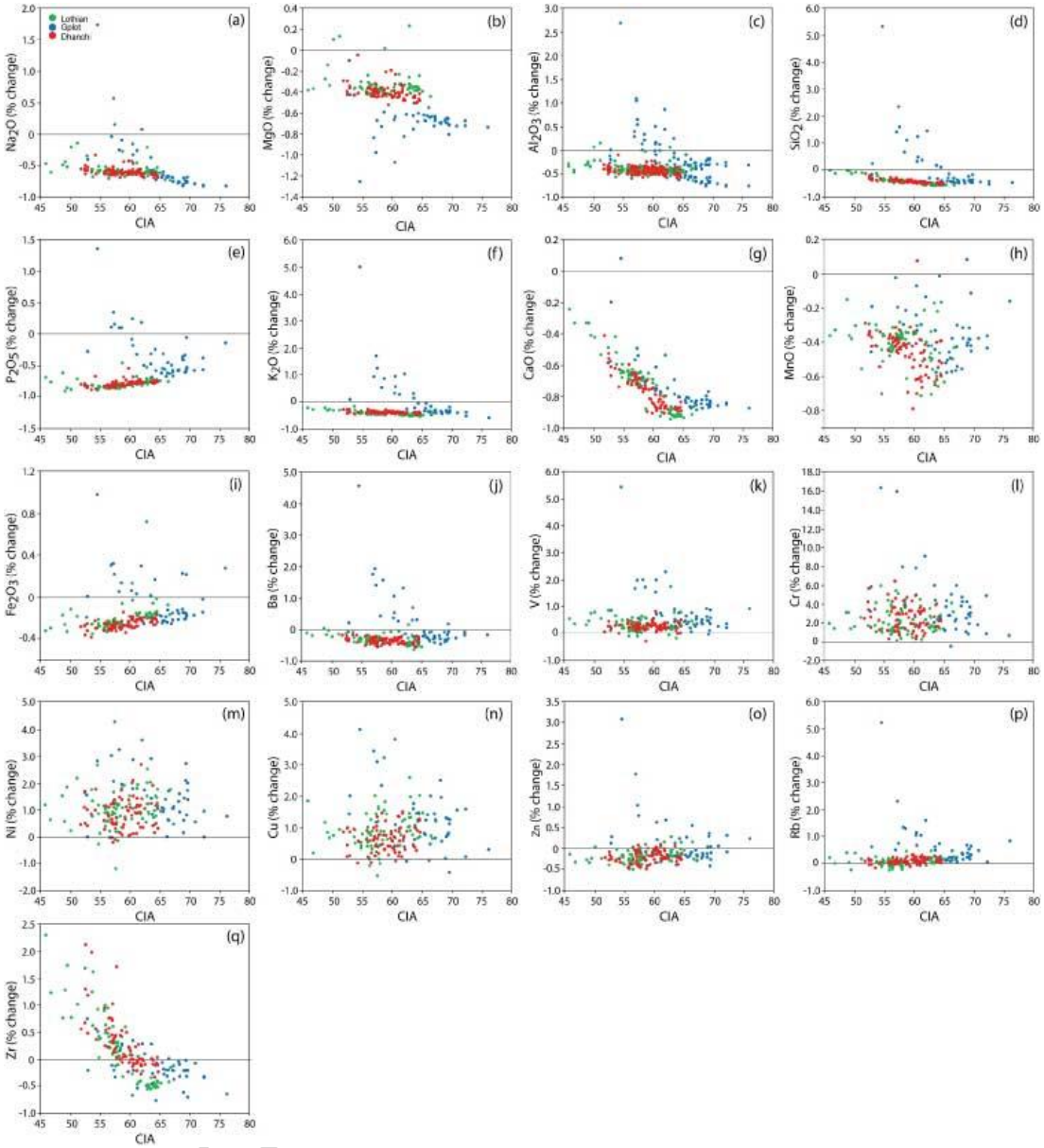

Fig. 12

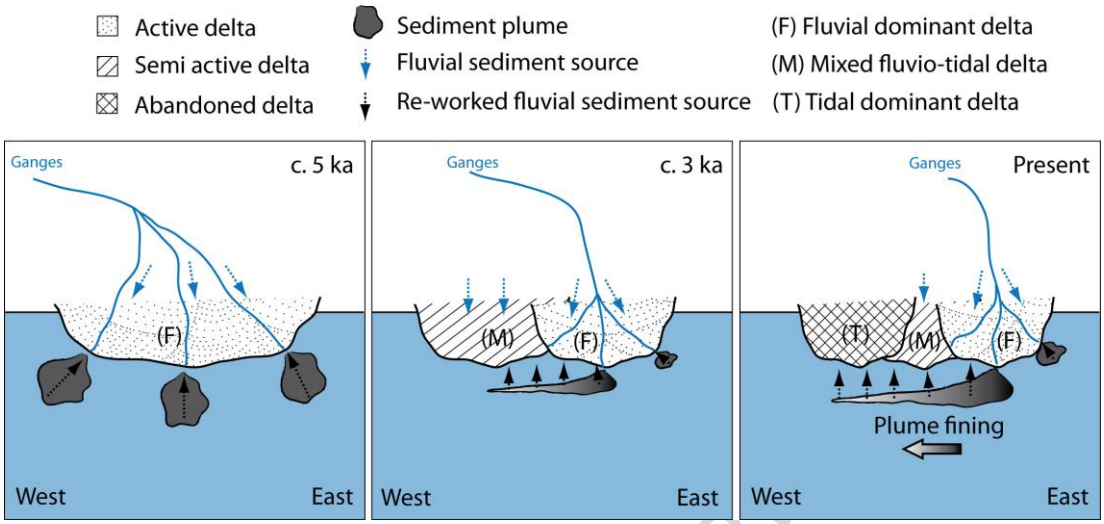

Fig. 13

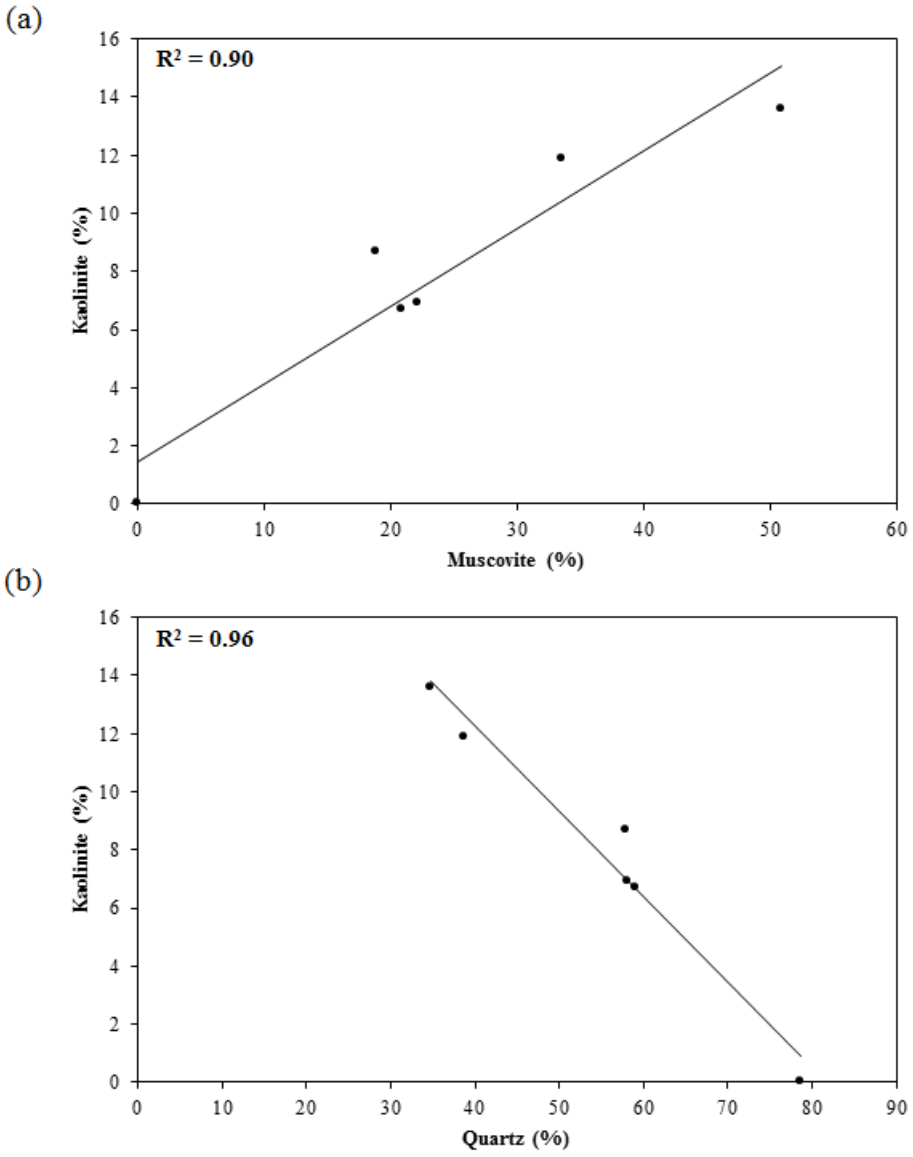

Fig. 14

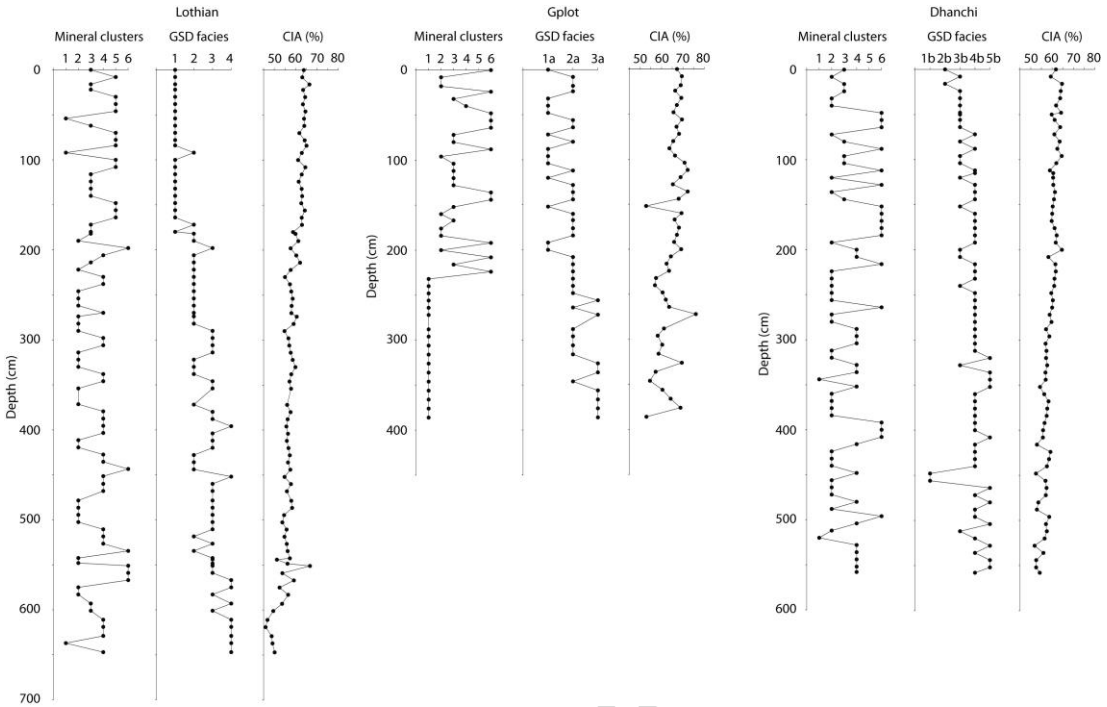

Fig. 15

Table 1

Principal component	Initial Eigenvalues			Extraction Sums of Squared Loadings		
	Total	% of Variance	Cumulative %	Total	% of Variance	Cumulative %
1	17.859	71.436	71.436	17.859	71.436	71.436
2	3.633	14.531	85.966	3.633	14.531	85.966
3	1.840	7.360	93.327	1.840	7.360	93.327
4	0.523	2.090	95.417	0.523	2.090	95.417

Table 2

Principal component	Initial Eigenvalues			Extraction Sums of Squared Loadings		
	Total	% of Variance	Cumulative %	Total	% of Variance	Cumulative %
1	10.294	85.787	85.787	10.294	85.787	85.787
2	1.008	8.399	94.186	1.008	8.399	94.186
3	0.622	5.181	99.367	0.622	5.181	99.367
4	0.048	0.4	99.767	0.048	0.4	99.767

Table 3

Site	Depth (cm)	Cluster group
Gplot Island	356	1
Dhanchi Island	456	2
Lothian Island	22	3
Dhanchi Island	304	4
Lothian Island	78	5
Dhanchi Island	184	6

Table 4

Statistic (%)	Cluster 1	Cluster 2	Cluster 3	Cluster 4	Cluster 5	Cluster 6
Rp	8.728	5.551	7.126	15.295	9.134	6.168
Weighted Rp	12.766	7.631	9.901	24.955	13.055	9.253
Rexp	4.271	4.038	4.251	4.569	4.418	4.043
X2	8.932	3.571	5.425	29.831	8.731	5.237
D-statistic	0.491	0.438	0.594	0.229	0.432	0.355
Weighted D-statistic	0.318	0.421	0.375	0.176	0.338	0.342

Table 5

	Quartz	Muscovite	Albite	Microcline	Clinochlore	Kaolinite	Dickite	Vermiculite
Cluster 1	58	18.8	10.4	0	4.2	8.7	0	0
Cluster 2	34.8	50.9	0	0	0	13.6	0	0.7
Cluster 3	58.2	22.1	10.2	0	2.7	6.9	0	0
Cluster 4	78.6	0	7.7	8.2	0.9	0	4.6	0
Cluster 5	59	20.9	13	0	0	6.7	0	0.4
Cluster 6	38.8	33.6	10.1	0	5.5	11.9	0	0

Table 6

Cluster	Mineralogical characteristics
Cluster 1	Relatively high quartz, muscovite, albite and clinochlore; moderate kaolinite abundance; absence of vermiculite, dickite, microcline.
Cluster 2	Relatively high muscovite and kaolinite; low quartz and possibly low vermiculite, absent of clinochlore, albite, dickite, microcline.
Cluster 3	Relatively high quartz, muscovite, albite; relatively high clinochlore, kaolinite and absent of vermiculite, dickite, microcline.
Cluster 4	High quartz content; relatively high microcline, and dickite; low albite and clinochlore; absence of muscovite and kaolinite.
Cluster 5	Relatively high quartz, muscovite, and albite content; low kaolinite content; absence of clinochlore, vermiculite, microcline, dickite.
Cluster 6	Relatively high muscovite, kaolinite, clinochlore and albite content; relatively low quartz content; complete absence of vermiculite, dickite, microcline.

Highlights

- Holocene TMF in the West Bengal Sundarbans determined to show intensively weathered, terrestrial sediment derived from the Ganges Alluvial Plain (GAP)
- Lithofacies is indicative of muddy tidal flat with aggradation and fining-up in grain size.
- Sediment provenance indicates a continuing G-B sediment source from the active delta front, with sediment reworked over the far-western abandoned delta by tidal–estuarine forcing.